



HAL
open science

Spectral Induced Polarization Response of Bacteria Growth and Decay in Soil Column Experiments

Yalin Song, Xiaoqing Shi, André Revil, Ahmad Ghorbani, Siyuan Qiang, Kun
Xing, Xueyuan Kang, Qilin Wang, Jichun Wu

► **To cite this version:**

Yalin Song, Xiaoqing Shi, André Revil, Ahmad Ghorbani, Siyuan Qiang, et al.. Spectral Induced Polarization Response of Bacteria Growth and Decay in Soil Column Experiments. *Journal of Geophysical Research: Biogeosciences*, 2024, 129 (12), pp.e2024JG008050. 10.1029/2024jg008050 . hal-04860139

HAL Id: hal-04860139

<https://hal.science/hal-04860139v1>







Submitted on 8 Jan 2025

HAL is a multi-disciplinary open access archive for the deposit and dissemination of scientific research documents, whether they are published or not. The documents may come from teaching and research institutions in France or abroad, or from public or private research centers.

L'archive ouverte pluridisciplinaire **HAL**, est destinée au dépôt et à la diffusion de documents scientifiques de niveau recherche, publiés ou non, émanant des établissements d'enseignement et de recherche français ou étrangers, des laboratoires publics ou privés.

Copyright

Spectral Induced Polarization Response of Bacteria Growth and Decay in Soil Column Experiments

Yalin Song¹ , Xiaoqing Shi¹ , André Revil² , Ahmad Ghorbani³, Siyuan Qiang¹ , Kun Xing¹, Xueyuan Kang¹, Qilin Wang⁴ , and Jichun Wu¹ 

¹Key Laboratory of Surficial Geochemistry of Ministry of Education, School of Earth Sciences and Engineering, Nanjing University, Nanjing, China, ²Université Savoie Mont-Blanc, CNRS, UMR CNRS 5204, EDYTEM, Le Bourget-du-Lac, France, ³Naga Geophysics, Technolac, Le Bourget du Lac, France, ⁴State Key Laboratory of Pollution Control and Resource Reuse, School of Environment, Nanjing University, Nanjing, China

Key Points:

- The growth and decay of gram-positive and gram-negative bacteria in soils exhibit a clear signature on their complex conductivity spectra.
- The spectra are fitted by a double Cole-Cole model, and the Maxwell-Wagner polarization is removed.
- The normalized chargeability and the Cole-Cole relaxation time vary linearly with the density of bacteria in the soil.

Correspondence to:

X. Shi,
shixq@nju.edu.cn

Citation:

Song, Y., Shi, X., Revil, A., Ghorbani, A., Qiang, S., Xing, K., et al. (2024). Spectral induced polarization response of bacteria growth and decay in soil column experiments. *Journal of Geophysical Research: Biogeosciences*, 129, e2024JG008050. <https://doi.org/10.1029/2024JG008050>

Received 28 FEB 2024
Accepted 27 NOV 2024

Author Contributions:

Conceptualization: Yalin Song, Xiaoqing Shi, André Revil, Ahmad Ghorbani, Jichun Wu
Data curation: Yalin Song
Formal analysis: Yalin Song, Xiaoqing Shi, Xueyuan Kang, Qilin Wang
Funding acquisition: Xiaoqing Shi, Jichun Wu
Investigation: Yalin Song, Xiaoqing Shi, Qilin Wang
Methodology: Yalin Song, Xiaoqing Shi, André Revil, Ahmad Ghorbani, Kun Xing, Xueyuan Kang, Qilin Wang, Jichun Wu
Project administration: Xiaoqing Shi
Resources: Xiaoqing Shi
Software: Yalin Song, Xiaoqing Shi, André Revil, Ahmad Ghorbani, Siyuan Qiang, Kun Xing, Xueyuan Kang, Qilin Wang
Supervision: Xiaoqing Shi, Jichun Wu
Validation: Yalin Song, Xiaoqing Shi, André Revil, Ahmad Ghorbani, Siyuan Qiang, Xueyuan Kang, Qilin Wang
Visualization: Yalin Song
Writing – original draft: Yalin Song
Writing – review & editing: Xiaoqing Shi, André Revil

Abstract Spectral induced polarization (SIP) exhibits potential to be a nonintrusive approach to monitor bacterial activity in biological hotspots associated with the critical zone of the earth. The polarization of bacteria in a low-frequency electrical field is related to the polarization of their electrical double layer coating their surface. However, few studies have quantified the induced polarization responses on both gram-negative (GN) and gram-positive (GP) bacteria in soil column experiments. To address this gap, 17 experiments using two strains, *Pseudomonas aeruginosa* O1 (PAO1, GN) and *Brevibacillus centrosporus* (L3, GP) are conducted. Complex conductivity spectra are collected in the frequency range 10 mHz–10 kHz during bacterial growth and decay phases in soils. The complex conductivity spectra are fitted using a double Cole-Cole model to remove the effect of Maxwell-Wagner polarization. The change in the magnitude of the polarization (quadrature conductivity or normalized chargeability of the low-frequency contribution) is linearly related to the bacterial density, regardless of the type of bacteria. The changes in the normalized chargeability and Cole-Cole relaxation time are directly proportional to the density of bacteria. Furthermore, it is inferred that the thickness of microcolonies plays a critical role in the relaxation time rather than the diameter of individual bacteria. This study expands the potential of SIP for in situ monitoring of microbial activity in soils.

Plain Language Summary Microorganisms are ubiquitous in the environment. Understanding their impact on the critical zone is crucial in the context of climate change. Spectral induced polarization is a geophysical method that has been proven to be sensitive to the presence of bacteria in porous media, but no specific works have been done for both gram-negative and gram-positive bacteria in soils. Column reactor experiments are conducted using the same soil, inoculated with either gram-negative or gram-positive strains. Experimental results indicate a direct proportionality between the magnitude of the low-frequency electrical polarization of the soil and the density of bacteria. It is inferred that the size of microcolonies plays a critical role in the value of the relaxation time. This study provides new quantitative insights into the relationship between the electrical properties and bacterial activity in soils with applications to the nonintrusive monitoring of biological hotspots in the critical zone of the earth.

1. Introduction

The important role of bacteria in various biogeochemical processes occurring in the critical zone of the earth have been thoroughly documented in the literature (Atekwana et al., 2006). For instance, microbially mediated reactions can significantly enhance the in situ biodegradation of organic contaminants in groundwater (Kimak et al., 2019; Personna et al., 2013). Effective monitoring and quantification of microbial growth and decay rates is crucial for predicting the efficiency of organic matter degradation through microbially mediated processes in aquifers (McCarty et al., 1981; Schultz and Urban, 2008). Conventional methods of microbial analysis in porous media generally rely on in situ sampling, which is limited by both temporal and spatial resolution among other issues (e.g., Douterelo et al., 2016). Additionally, these methods may disrupt subtle redox-sensitive biogeochemical processes because bacteria are often located on the surface of the grains rather than in the pore water (Borch et al., 2010; Griebler & Lueders, 2009). Therefore, noninvasive monitoring of microbial activity is essential for understanding microbially mediated reactions in porous media.

In recent years, spectral induced polarization (SIP) has emerged as a viable, nonintrusive, and qualitative approach to explore changes in the complex conductivity of rocks and soils (e.g., Abdel Aal et al., 2004, 2006; Martin

et al., 2022; Olhoeft, 1985; Panwar et al., 2021; Revil, 2012; Saneiyani and Slater, 2021; Schwartz and Furman, 2012; Vinegar and Waxman, 1984). This geophysical method is also currently used to monitor the remediation of organic pollution plumes in groundwater environments (Deng et al., 2018, 2020; Orozco et al., 2015, 2021). In porous media, in the absence of metallic particles and within the low-frequency range (1 mHz–1 kHz), charge storage is primarily controlled by the polarization of the electrical double layer (EDL) surrounding the charged surfaces of minerals, especially clay minerals (e.g., Leroy & Revil, 2009; Vanhala et al., 1992). The EDL consists of an inner Stern layer surrounded by the so-called (Gouy-Chapman) diffuse layer (e.g., Oldham, 2008).

The polarization of bacteria is considered analogous to the polarization of clay particles by Revil, Atekwana, et al. (2012). This is because the surface of bacteria contains charged functional groups with complexation reactions giving birth to a surface charge density like in clay minerals. For bacteria, Stern layer polarization and surface conduction within the polymeric brush layer drive significant charge storage, resulting in a high value of the quadrature conductivity (Poortinga et al., 2002; Revil, Atekwana, et al., 2012). Consequently, microbes present in a soil can be conceptualized as additional particles contributing to the overall complex conductivity of the mixture (Mellage et al., 2019; Revil, Atekwana, et al., 2012; Sanchis et al., 2007; Strobel et al., 2023). Various authors have demonstrated that SIP represents a viable technique for monitoring bacterial activities in porous media (e.g., Abdel Aal et al., 2009; Atekwana, Atekwana, Legall, & Krishnamurthy, 2004; Atekwana, Atekwana, Rowe, et al., 2004; Atekwana, Atekwana, Werkema, et al., 2004; Atekwana & Slater, 2009). Rosier et al. (2019) and Zhang et al. (2014) have connected the SIP responses to the density of bacteria in colloidal suspensions of bacteria. Davis et al. (2006) and Ntarlagiannis et al. (2005) have shown the dependence of quadrature conductivity on bacterial density in sands. Furthermore, Mellage et al. (2018, 2019) have evidenced a linear relationship between the change in the quadrature conductivity and the density of bacteria in a pure silica-based sand. Even under high-salinity conditions, bacterial activities can be effectively monitored using SIP (Joo et al., 2021). However, soils are complex media, and the presence of clays can also enhance their induced polarization response (Revil, Ghorbani, Jougnot, & Yven, 2023; Revil, Ghorbani, Jougnot, Yven, Grgic, et al., 2023; Revil et al., 2021). Recently, Song et al. (2022) conducted laboratory experiments to monitor the growth and decay of the bacteria in natural soil columns, in which the presence of clays in the overall polarization response of the mixture was considered. Based on the complex conductivity data obtained from SIP and the in situ bacterial density, a linear physics-based quantitative relationship was established between the quadrature conductivity and the density of bacteria.

Previous studies have only focused on GN bacteria (Abdel Aal, Atekwana, & Atekwana, 2010; Abdel Aal, Atekwana, Rossbach, & Werkema, 2010; Joo et al., 2021; Mellage et al., 2018; Rosier et al., 2019; Song et al., 2022; Zhang et al., 2014), and both GN and GP bacteria can be found in natural habitats of the critical zone of the earth (e.g., Tong et al., 2010). It is understood that the induced polarization of soils is sensitive to their cation-exchange capacity (CEC, see for instance Revil et al., 2013). The CEC denotes the amount of exchangeable cation on its surface per unit mass of grains (Revil et al., 2014). It can be measured through potentiometric titrations, for example, using the cobalthemanine method (Aran et al., 2008). The CEC of a specific strain of bacteria may be distinctive due to the unique surface density of counterions on the bacterial surface (Van der Wal et al., 1997). The surfaces of GP and GN bacteria contain peptidoglycan and lipopolysaccharides polymers, respectively. The peptidoglycan chain in GP bacteria is rich in three types of reactive charged surface groups: carboxylic acid, amine, and phosphate. In contrast, the GN bacteria contain charged phosphate and carboxyl groups (Leone et al., 2007). The CEC value of the bacteria typically ranges from 16 to 600 cmol/kg (1 cmol/kg = 1 meq/100 g), and generally, the CEC of GP bacteria is typically higher than that of GN bacteria (Dittrich & Sibling, 2005; Hadjoudja et al., 2010; Revil, Atekwana, et al., 2012; Walker et al., 2005). Previous studies have demonstrated that quadrature conductivity can be influenced by CEC as it enhances EDL polarization due to increased ionic exchange and storage at the surface of bacteria or clay particles (Okay et al., 2014; Revil, 2013; Weller et al., 2013). Therefore, it is of great importance to evaluating the electrical responses of both GN and GP bacteria.

In order to interpret complex conductivity spectra, the Cole-Cole complex conductivity model can be used as a parametric model to fit the complex conductivity spectra (Cole & Cole, 1941). The model assumes that the distribution of the polarization length scales responsible for the distribution of the relaxation time can be approximated by a log-normal distribution (Cole & Cole, 1941; Revil, Ghorbani, Jougnot, & Yven, 2023). Analyzing the relationship between Cole-Cole parameters and bacterial density is a key aspect to reveal how the SIP response is sensitive to the bacterial density. In previously published studies, conflicting evidence about whether bacterial density affects the relaxation time or not is noted. For instance, no correlation between the density of bacteria (without porous media) and the relaxation time was found in the case of colloidal suspension of

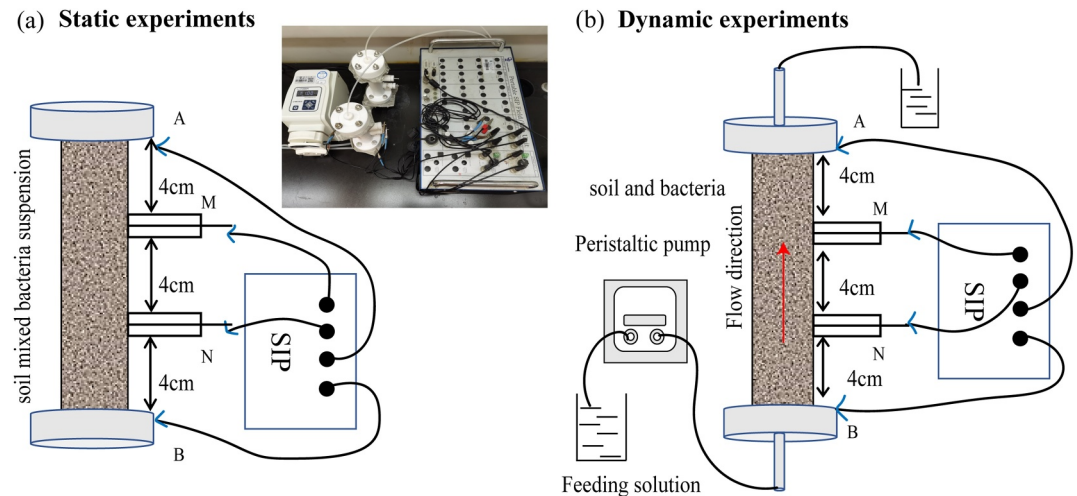


Figure 1. Sketch of the experimental setup. (a) and (b) represent the static and dynamic experiments, respectively. A portable spectral induced polarization is used to collect complex conductivity spectra (modified from Song et al. (2022)). (a) A and (b) are the (stainless steel) current electrodes while *M* and *N* represent the voltage electrodes. The geometric factor *K* used to convert the impedance into complex conductivity is given by $K = L/A = 127.38 \text{ m}^{-1}$, where $L = 4 \text{ cm}$ denotes the distance between the *M* and *N*, and *A* denotes the cross-sectional area of the soil column.

bacteria (Rosier et al., 2019), likely suggesting that the polarization is associated with individual bacteria. However, a decrease in the relaxation time with an increase in the number of inoculated bacteria with silica sand was observed by Joo et al. (2021). However, both these results were interpreted with the single Cole-Cole model. A double Cole-Cole complex resistivity model was employed by Strobel et al. (2023) to distinguish the matrix polarization (without bacteria) and bacteria-related polarization. However, in Strobel et al. (2023), the fitting results for the relaxation times were still affected by Maxwell-Wagner polarization due to the frequency at which the complex conductivity spectra was measured (1 kHz). Generally, the Maxwell-Wagner polarization typically appears in the frequency range from 10^3 to 10^6 Hz (Ferris et al., 1990; Irirajiri et al., 1987). It was shown from recent studies that Maxwell-Wagner polarization can actually be observed at 100 Hz and sometimes even be dominating at lower frequency (1–10 Hz) when the CEC of the background material is low (Cheng et al., 2024; Revil et al., 2018). The use of the double Cole-Cole model was discussed for instance by Revil, Ghorbani, Jougnot, and Yven (2023) and Revil, Ghorbani, Jougnot, Yven, Grgic, et al. (2023), as a way to remove the Maxwell-Wagner contribution. To date, there has been no investigation of using double Cole-Cole model to separate the contribution of the induced polarization (soil plus bacteria) from the Maxwell-Wagner polarization since the two are overlapped at low frequency. Since there is a superposition of the spectra associated with both mechanisms, it is essential to distinguish the two polarization mechanisms to ensure that Cole-Cole parameters variations are only associated with the low-frequency-induced polarization of the soil plus the bacteria.

2. Materials and Methods

2.1. Experimental Setup

12 cm-long polytetrafluoroethylene (PTFE) columns with an inner diameter of 2 cm were used, and two filters with a pore diameter of 0.074 mm were placed at the ends of these columns. Two Ag-AgCl potential electrodes *M* and *N* were placed between the current stainless-steel electrodes *A* and *B* (Figure 1) in chambers fitted through the sides of the column. A peristaltic pump (Longer pump, L100-1S-2) at an initial flow rate of 1 mL/min was used to continuously feed the soil-packed columns with sterilized growth media. A sketch of the experimental setup is shown in Figure 1. Both static and dynamic experiments were conducted in this study (labeled C1–C17, Table 1). Static experiments involved maintaining the columns in a stationary state, ensuring no interference from water flow. In contrast, the dynamic experiments involved continuously injecting a feeding solution into the columns to simulate real groundwater flow scenarios and monitor the growth and decay of bacteria.

Figure 1a showed the setup for the static experiment. SIP measurements were undertaken with the soil alone at three different salinities to determine the formation factor *F* (dimensionless) and surface conductivity σ_s (in

Table 1
The Study Included a Total of 17 Experiments (Labeled C1–C17),
Comprising Both Static and Dynamic Experiments

Columns	Types	Bacteria	Purposes
C1	Static	–	SIP measurement
C2	Static	–	SIP measurement
C3	Static	–	SIP measurement
C4	Dynamic	PAO1	SIP measurement
C5	Dynamic	PAO1	SIP measurement
C6	Dynamic	PAO1	Bacterial density
C7	Dynamic	PAO1	Microcolonies thickness
C8	Dynamic	PAO1	Microcolonies thickness
C9	Dynamic	PAO1	Microcolonies thickness
C10	Dynamic	PAO1	Microcolonies thickness
C11	Dynamic	PAO1	Microcolonies thickness
C12	Dynamic	PAO1	CEC measurement
C13	Dynamic	PAO1	CEC measurement
C14	Dynamic	L3	SIP measurement
C15	Dynamic	L3	SIP measurement
C16	Dynamic	L3	Bacterial density
C17	Control	–	SIP measurement

$S\ m^{-1}$) of the soil itself (C1–C3). Figure 1b showed the setup of dynamic experiments involving active and control scenarios (C4–C17). For each type of bacteria, two columns were used in duplicate for monitoring the bacterial growth and decay by SIP (labeled C4 and C5 for PAO1, C14 and C15 for L3), while a third column was used for bacterial density analysis (labeled C6 for PAO1, C16 for L3). Additionally, for GN bacteria, there were five columns sacrificed at different time points for microcolonies thicknesses (labeled C7–C11) and two columns sacrificed for CEC measurements (labeled C12 and C13). A control experiment was performed with the soil in absence of any bacteria in it (labeled C17). All columns, tubing, and accessories were sterilized by rinsing them with ethanol (75%) prior to the experiments. Reactors were sealed with polytetrafluoroethylene (PTFE) screw end caps at either ends, fitted with inflow and outflow channels at the bottom and the top, respectively.

2.2. Bacteria and Growth Media

To test the polarization of different types of bacteria, two typical strains were selected. *Pseudomonas aeruginosa* O1 (labeled PAO1 hereinafter) was a typical GN strain, which was commonly present in groundwater and cultivated here to form microcolonies. Microcolonies are small clusters of bacteria that form during bacterial growth, typically consisting of a few hundred individual bacteria (Torrella and Morita, 1981; Zhao et al., 2013). The strains were obtained from the China General Microbiological Culture Collection Center, CGMCC (strain number 1.12483). A GP strain, *Brevibacillus centrosporus* (strain L3), was isolated from the soil (Nanjing, China). The CEC

of PAO1 is 46 cmol/kg live cells under neutral pH values (Shephard et al., 2008), whereas the CEC of L3 is 348 cmol/kg live cells at neutral pH (Van der Wal et al., 1997). It should be noted that the CEC per gram of dry bacteria to the CEC per gram of hydrated bacteria was converted by using a dry weight to wet weight ratio W of 0.5 (Walker et al., 2005). The Luria-Bertani (LB) medium (10 g/L peptone, 5 g/L yeast extract, and 10 g/L sodium chloride) was used to propagate bacteria in large quantities. The feeding solution employed in soil columns experiments comprises 25% Bushnell Hass broth (BHB) supplemented with 30 mM glucose to serve as a carbon source (Abdel Aal, Atekwana, & Atekwana, 2010; Abdel Aal, Atekwana, Rossbach, & Werkema, 2010; Davis et al., 2006). The ingredient of 25% BHB was shown in Table 2 with the conductivity of $0.107 \pm 0.001\ S\ m^{-1}$ at 25°C. For the control experiment, a 0.05% sodium azide (pore water solution) was used to prevent the presence of bacteria.

2.3. Experimental Procedure

For the dynamic experiments, the bacteria were cultured in an LB medium until the logarithmic phase was reached (placed on a rotary shaker at 130 rpm and the temperature of 30°C), and then, the bacteria were collected after centrifuging at 8,000 rpm for 10 min and rinsed with 25% BHB to remove the remaining LB medium. Subsequently, the bacterial suspension was used to wet pack the soil columns. Soil porosity ($\phi = 0.35 \pm 0.02$) was determined by dividing the volume of solution used during multiple wet packing by the volume of the column prior to the experiments. After packing the column, the feeding solution was pumped into the column to start the growth phase, and the SIP measurements were conducted at different time intervals. However, it should be noted that at the initial stage of the experiment, the majority of bacteria are carried out with the pore water flow from the outlet, while only a very few bacteria adhere to the soil grain surface and begin to grow, leading to a relatively low bacteria density at the beginning (temperature, $T = 25^\circ C$) (Cui et al., 2021; Sen, 2011; Stevik et al., 2004).

Table 2
Chemical Composition of 25% (Mass Concentration) Bushnell Hass Broth
Used as a Nutrient Solution for the Growth of Bacteria

Compound	Concentration (g/L)
MgSO ₄	0.05
CaCl ₂	0.005
KH ₂ PO ₄	0.25
K ₂ HPO ₄	0.25
KNO ₃	0.25
FeCl ₃	0.0125
Glucose	5.4

Note. The electrical conductivity of this solution is $0.1065\ S\ m^{-1}$ at 25°C.

2.4. Bacteria Density and CEC Analysis

During the bacterial growth and decay phases, the bacterial density, which referred to the quantity of the bacteria absorbed on the surface of the soil grain, was analyzed at different time intervals (Bellin & Rao, 1993; Cui et al., 2023). Samples for measuring bacterial density were taken at 4 cm away from the inlet of columns C6 and C16. Approximately 0.5 g wet soil was extracted at different time intervals during the growth and decay phases (Davis et al., 2006; Ntarlagiannis et al., 2005; Song et al., 2022). The soil was then sufficiently washed with 10 ml sodium chloride at a concentration of 0.85%. Subsequently, bacterial density was determined using the dilution plate method to count the number of bacteria (Jett et al., 1997). Here, the PAO1 and L3 were cultivated, respectively, on the agar LB medium and the ISP2 medium (Arumugam, 2017).

The CEC of soil during the bacterial growth phase was measured using the hexaamminecobalt trichloride solution, following the spectrophotometric method recommended in the environmental protection standards of the People's Republic of China (HJ 889-2017, see Tan et al., 2018; Xu et al., 2022). Hexaamminecobalt trichloride solution was mixed with the soil extracted from the active column in a centrifuge tube, obtaining a nearly neutral pH at about 6.9, which was then placed in the centrifuge tube into an oscillator and shaken for about 60 min. During this operation, the environment was suitable for bacteria growth. Therefore, the CEC of soil containing the bacteria was measured representing that in the mixed clay minerals and the bacteria.

2.5. The Visualization of Bacteria on Soil and Thickness

At the end of the experiments, the soil samples extracted from the columns were imaged using scanning electron microscopy (SEM, Zeiss Sigma 500 electron microscopy) to investigate the evidence of bacteria attached on the soil. The fixation of samples and preparation for SEM were as follows (Cen et al., 2004): the soil samples mixed with bacteria were firstly washed with phosphate buffer solution (PBS) immediately after the incubation period; then, 3 vol% glutaraldehyde in PBS was added for 5 hr and stored at 4°C. The glutaraldehyde solution was then removed, and the substrates were washed with PBS, followed by step dehydration with 25%, 50%, 70%, 95%, and 100% ethanol for 10 min each. The substrates were then dried and sputter-coated with a thin film of platinum for imaging purpose. The SEM characterization was carried out using Zeiss Sigma 500 SEM.

The SEM can only image the contour of bacteria but cannot capture the dynamic changes in the thicknesses of microcolonies. Therefore, confocal laser scanning microscopy (CLSM) has been introduced as a new, nondestructive analytical method that provides a better understanding of the size of microcolonies. Furthermore, CLSM has the potential to analyze live biological samples, particularly thick samples. Therefore, microorganisms can be detected in situ by an appropriate staining method by CLSM analysis (Takenaka et al., 2001).

Before measuring the thickness of microcolonies, the living bacteria were stained with Annexin V-FITC, which was characterized by a green color (Eray et al., 2001). The samples were prepared based on the manual of Annexin V-FITC as described below: A column was sacrificed and soil samples were taken at different time intervals. The samples were washed thrice with PBS, emerged with 5 μ L of Annexin V-FITC solution in darkness for 15 min, washed again with PBS, and finally placed on a glass slide under the cover glass. They were then ready for scanning under the CLSM. The step size of CLSM was set to 5 μ m, and the thicknesses of microcolonies were calculated by the photo of the fluorescence strength. The sampling time intervals during the growth phase were set at 1,160 min and 4,150 min, while during the decay phase, they were set at 4,190 min, 4,300 min, and 4,420 min. The sampling points were located at 1, 2, 3, 4, 5, and 6 cm from the inlet of soil columns (Figure 1). It should be noted that the bacteria near the inlet have received the nutrients first, leading to a higher population of bacteria close to the inlet (Cui et al., 2023).

2.6. SIP Measurements

The potential electrodes were in electrical contact with the soil matrix but not extended into the column to minimize spurious polarization that can develop at the electrode surface in the current distribution generated in the soil column. A portable SIP device (Ontash and Ermac Inc., NJ) was used to obtain the impedance magnitude ($|Z|$) and the phase angle (φ) spectra in the frequency range from 0.01 Hz to 10 kHz at 40 equal logarithmic intervals. The in-phase σ' and quadrature conductivity σ'' spectra of the complex conductivity are then obtained from the impedance and phase spectra plus a geometrical coefficient K (Figure 1) depending on the position of the electrodes. The term K is the geometric factor (expressed in m^{-1}), depending on the geometry of the electrodes, the shape of the

conductive material, and boundary conditions. For the simple ABMN electrode configuration (Figure 1), K is calculated as $L/A = 127.38 \text{ m}^{-1}$, where L denotes the distance between electrodes M and N , and A denotes the cross-sectional area of the soil column where the current flows.

The in-phase and quadrature conductivity are related to the impedance Z and the phase by the following:

$$\sigma' = \frac{K}{|Z|} \cos \varphi = \frac{L}{A|Z|} \cos \varphi, \quad (1)$$

$$\sigma'' = \frac{K}{|Z|} \sin \varphi = \frac{L}{A|Z|} \sin \varphi, \quad (2)$$

The first step of the analysis is to separate the induced polarization signals of the soil plus bacteria from the Maxwell-Wagner polarization because both overlap in a broad range of frequencies (Revil, Ghorbani, Jougnot, & Yven, 2023; Revil, Ghorbani, Jougnot, Yven, Grgic, et al., 2023; Revil et al., 2013). The complex conductivity spectra are therefore fitted with a double Cole-Cole model (Revil, Ghorbani, Jougnot, & Yven, 2023; Revil, Ghorbani, Jougnot, Yven, Grgic, et al., 2023; Revil et al., 2019):

$$\sigma^* = \sigma_{\infty} - \frac{M_n^1}{1 + (i\omega\tau_1)^{c_1}} - \frac{M_n^2}{1 + (i\omega\tau_2)^{c_2}}, \quad (3)$$

where 1 and 2 in the superscript and the subscript are referred to lower and higher frequency dispersions, respectively. The low-frequency polarization corresponds to the induced polarization of the bacteria and the soil together while the high-frequency polarization represents the Maxwell-Wagner polarization. The quantities M_n^1 and M_n^2 (S m^{-1}) denote the normalized chargeability, c_1 and c_2 (dimensionless) are the two Cole-Cole exponents, and τ_1 and τ_2 (in s) are the Cole-Cole relaxation times. However, it is important to note that the double Cole-Cole model here differs from that in Strobel et al. (2023) because Strobel et al. (2023) employed the complex resistivity model to distinguish the matrix and bacteria polarization. In contrast, this study used the complex conductivity model by separating the low-frequency component associated with bacteria and soil polarization from the high-frequency component related to Maxwell-Wagner polarization, which is associated with the discontinuity of the displacement current at the interfaces of the porous composite. In addition, double Cole-Cole complex resistivity and complex conductivity models are not equivalent.

The second step is to analyze the response associated with the induced polarization signals of the soil plus bacteria. Thus, the induced polarization signals could be considered as the sum of the responses of the soil plus the response associated with the bacteria. The former is static, remaining stable over time, while the response associated with the bacteria is dynamic. To keep the response associated with the bacteria alone, the complex conductivity response measured at the beginning of the experiment, when the bacterial count is negligible, can be easily removed. It should be noted that several soil samples at different saturations were used, so the initial response may be different at the beginning from one experiment to the other. The normalized chargeability associated with induced polarization of a soil in unsaturated conditions can be written as follows (Revil, Karaoulis, et al., 2012; Revil et al., 2017):

$$M_n^1 = \frac{s_w^{n-1}}{F} \lambda Q_v, \quad (4)$$

where s_w (dimensionless) is the liquid pore water saturation, F (dimensionless) is the intrinsic formation factor, $n > 1$ (dimensionless) denotes the saturation exponent, and Q_v denotes the (volumetric) charge density of the counterions per unit pore volume associated with the CEC exposed to the pore space by the clay minerals. The mobility λ (Na^+ , 25°C) = $3.0 \pm 0.7 \times 10^{-10} \text{ m}^2 \text{ s}^{-1} \text{ V}^{-1}$ denotes the apparent mobility of the counterions in the EDL for the polarization (Revil et al., 2017).

The polarization of a soil occurs primarily because of the presence of the clay minerals given their large CEC in the absence of metallic grains. The CEC represents the amounts of exchangeable cations at the surface of the clay particles. The presence of bacteria would however increase the CEC in the pore space of the soil. Therefore, the normalized chargeability of a soil with bacteria can be rewritten from Equation 4 as follows:

$$Q_V = Q_V(\text{soil}) + Q_V(\text{bacteria}), \quad (5)$$

where the two contributions associated with the clay minerals and the bacteria can be written as follows:

$$Q_V(\text{soil}) = \rho_g \left[\frac{1 - \phi}{\phi} \right] \varphi_C \text{CEC}_C, \quad (6)$$

$$Q_V(\text{bacteria}) = \rho_B \left[\frac{1 - \phi}{\phi} \right] \varphi_B \text{CEC}_B, \quad (7)$$

where ρ_g and ρ_B (kg m^{-3}) is the density of the grain and bacteria, respectively. φ_C and φ_B denote the mass fraction of clay minerals and bacteria, respectively, and CEC_C and CEC_B denote the CEC of the clay mineral and bacteria, respectively. The quantity ϕ is the porosity of the soil in which the bacteria grow. Obviously, $\varphi_B \sim \frac{C_B}{m_{\text{soil}}}$, C_B is the bacterial density, and m_{soil} is the weight of soil; thus, the normalized chargeability can be considered as the sum of those from background plus a contribution proportional to the normalized bacterial density.

If the soil polarization has been subtracted from the overall induced polarization response obtained at the end of step 1 (removing the Maxwell polarization), the low-frequency normalized chargeability can be written as follows:

$$M_n^1 = \frac{s_w^{n-1}}{F} \lambda \left[\frac{1 - \phi}{\phi} \right] \rho_B \varphi_B \text{CEC}_B, \quad (8)$$

and is therefore directly proportional to the density of bacteria φ_B .

The instantaneous conductivity denotes the conductivity of the material just after the application of the electrical field when all the charge carriers are mobile. The DC (direct current) conductivity denotes the value of the conductivity after a long application of the electrical field, when the charge associated with the polarization process are lost for conduction and therefore $\sigma_0 < \sigma' < \sigma_\infty$. The instantaneous conductivity associated with the soil plus bacteria can be written as (Revil, Karaoulis, et al., 2012; Revil et al., 2017) follows:

$$\sigma_\infty = \frac{s_w^n}{F} \left[\sigma_w + \frac{BQ_V}{s_w} \right]. \quad (9)$$

where B denotes the effective mobility of the counterions in the double layer ($B(\text{Na}^+, 25^\circ\text{C}) = 3.1 \pm 0.3 \times 10^{-9} \text{ m}^{-2} \text{ s}^{-1} \text{ V}^{-1}$, Revil et al., 2017) and σ_w (S/m) denotes the pore water conductivity. Because of the small dispersion of the in-phase conductivity with the frequency, the instantaneous conductivity is a good approximation of the in-phase conductivity. When the (instantaneous) conductivity is dominated by the bulk conductivity contribution (small clay fraction), the instantaneous conductivity is approximated by Equation 10 and is independent of the quantity of bacteria and clay minerals:

$$\sigma_\infty \approx \frac{s_w^n}{F} \sigma_w, \quad (10)$$

If the soil contribution is removed, the remaining excessive conductivity associated with the bacteria can be written as follows:

$$\sigma_\infty = B \frac{s_w^{n-1}}{F} \rho_B \left[\frac{1 - \phi}{\phi} \right] \varphi_B \text{CEC}_B, \quad (11)$$

Therefore, this excess conductivity is directly proportional to the density of bacteria as long as the porosity and water saturation remain constant. It is indicated that the conductivity contribution associated with the soil itself is usually much higher than the contribution associated with the bacteria. The effect of the bacteria is a second-order effect on the overall conductivity contribution. The effect of the bacteria on the normalized chargeability or the quadrature conductivity (both are proportional to each other and the relationship between the two is quantitative, Revil et al., 2017) is a first-order effect. Thus, it is easier to observe and monitor the effect of the bacteria through monitoring the polarization of the material rather than by monitoring its conductivity.

Table 3
Physical Properties of the Soil Used in the Column Experiments

Properties	Result
Soil composition (in weight)	85.34% sand, 12.63% silt, and 2.03% clay
Minerals	Quartz, albite, illite, and chlorite
Cation-exchange capacity	0.8 cmol/kg
Porosity	0.35 ± 0.02

For a suspension of bacteria, the Cole-Cole relaxation time τ (in s) is related to the mean size of the bacteria d_B (in m) as shown by the following equation (Revil, Karaoulis, et al., 2012):

$$\tau = \frac{d_B^2}{8D_{(+)}} \quad (12)$$

where $D_{(+)}$ (in $\text{m}^2 \text{s}^{-1}$) denotes the diffusion coefficient of the counterions in the Stern layer, which can be related to the mobility B (see Revil et al., 2021).

In presence of microcolonies inside a soil, it is possible that the polarization length scale is associated with the size of the microcolonies instead of the size of the single bacteria. This point will be extensively discussed later in this study.

2.7. Soil Properties Characterization

The soil used in this study was extracted from the Xinjiang Uygur Autonomous Region, China (85°54'E, 44°54'N), which was composed of 85.34% sand, 12.63% silt, and 2.03% clay (laser particle size analyzer, Shimadzu). The CEC of soil alone was also measured with the method of hexaamminecobalt trichloride and was approximately 0.8 cmol/kg. X-ray diffraction (XRD) tests were performed on a soil sample indicating that the soil composition include quartz, albite, illite, and chlorite. The porosity of the soil is 0.35 ± 0.02 (Table 3). The formation factor F and surface conductivity σ_s of the soil were obtained by collecting the SIP response under different salinities (Table 4). The in-phase conductivity can be fitted by the following equation:

$$\sigma' \approx \frac{\sigma_w}{F} + \sigma_s \quad (13)$$

The formation factor F and surface conductivity σ_s are determined using the logarithmic form of Equation 13 (El Alam et al., 2023; Revil et al., 2013). The estimated F and σ_s for the soil used in this study are 3.86 and 0.004 S m^{-1} , respectively (Figure 2).

3. Results

3.1. SIP Responses of Bacteria Growth and Decay

The variations of the in-phase and quadrature conductivity during the bacteria growth and decay, and the complex conductivity spectrum of the soil alone in absence of bacteria, are shown in Figure 3. The complex conductivity spectra are fitted with the double Cole-Cole model. As shown in Figures 3a and 3c, the in-phase conductivity does not exhibit strong change during the bacteria growth and decay. On the contrary, the quadrature conductivity changes during both bacterial growth and decay phases (Figures 3b and 3d). Figures 3e and 3f shows the in-phase and quadrature conductivity of the Xinjiang soil without any bacteria in it. The SIP responses from the control experiment were shown in Figure 4; however, no changes in quadrature and in-phase conductivity are observed. Figure 5 shows the phase changes of PAO1 and L3 and the control experiments. No changes are observed for the control experiment, whereas for PAO1 and L3, the phases are changed at different degrees. At the same time, the bacterial density, which represents the amounts of bacteria absorbed on the soil grain surface, is acquired at different time intervals and displayed with the variation of averaged quadrature conductivity in Figures 6a and 6b.

As shown in Figure 6a, the measured quadrature conductivity at the peak frequency is $7.62 \times 10^{-5} \text{ S m}^{-1}$ after 40 min into the experiment. As the bacterial growth continues, it is accompanied by a rise in quadrature conductivity. After 1260 min, the quadrature conductivity at peak frequency increases to $8.95 \times 10^{-5} \text{ S m}^{-1}$. Toward the end of the growth phase, the quadrature conductivity increases to $1.13 \times 10^{-4} \text{ S m}^{-1}$. The bacterial density on the grain surface of PAO1 increases from $3.75 \times 10^8 \text{ cells g}^{-1}$ to $4.26 \times 10^9 \text{ cells g}^{-1}$ during the growth phase. The SIP responses during bacterial decay are driven by the cessation of the feeding solution. During this phase, the quadrature conductivity significantly decreases, with the

Table 4
Pore Water Conductivity and Resulting In-Phase Conductivity Used to Determine the Intrinsic Formation Factor and Surface Conductivity of the Saturated Soil Without the Bacteria ($T = 25^\circ\text{C}$)

Pore water conductivity (S/m)	In-phase conductivity (S/m)
0.092	0.027
0.289	0.080
0.478	0.126

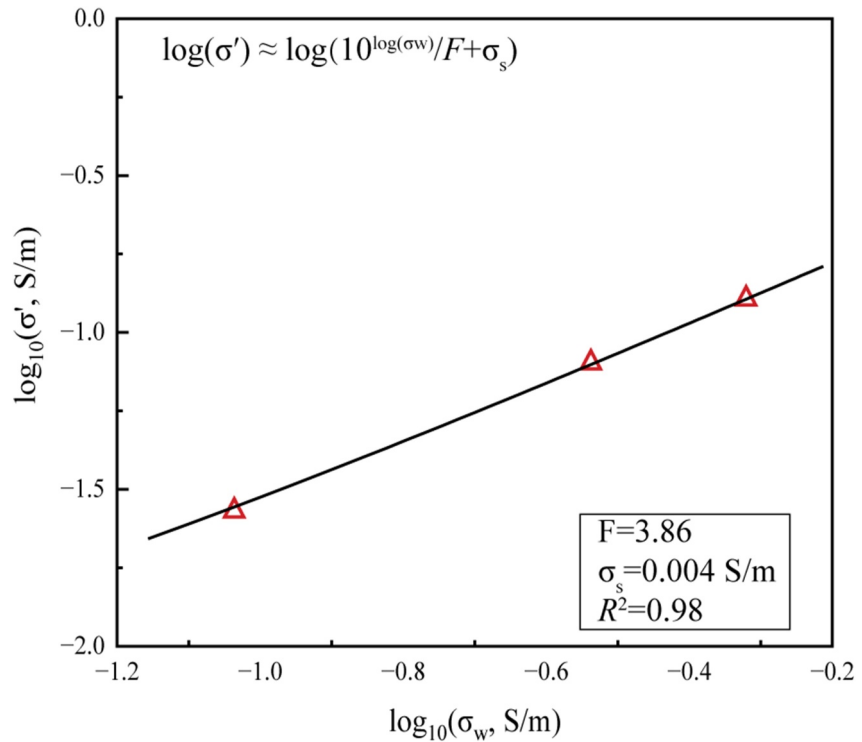


Figure 2. The in-phase (σ') conductivity (1 Hz) versus pore water conductivity σ_w (expressed in S/m). The solution was NaCl at three salinities ($T = 25^\circ\text{C}$).

quadrature conductivity at peak frequency declining from $1.13 \times 10^{-4} \text{ S m}^{-1}$ to $6.93 \times 10^{-5} \text{ S m}^{-1}$, representing a 39% decrease from the initial value during the decay of PAO1. Concurrently, the bacterial density of PAO1 decreases from $4.26 \times 10^9 \text{ cells g}^{-1}$ to $0.50 \times 10^9 \text{ cells g}^{-1}$.

The SIP responses during L3 growth and decay are shown in Figure 6b. The quadrature conductivity at peak frequency is measured at approximately $6.95 \times 10^{-5} \text{ S m}^{-1}$ after 40 min into the experiment. As the L3 grows, the quadrature conductivity increases to $8.51 \times 10^{-5} \text{ S m}^{-1}$ at 1650 min and subsequently to $1.20 \times 10^{-4} \text{ S m}^{-1}$ by the end of the experiment. During the growth phase, the bacterial density of L3 increases from $2.18 \times 10^7 \text{ cells g}^{-1}$ to $3.13 \times 10^9 \text{ cells g}^{-1}$. In contrast, during the decay phase, the quadrature conductivity at peak frequency decreases from $1.20 \times 10^{-4} \text{ S m}^{-1}$ to $8.7 \times 10^{-5} \text{ S m}^{-1}$, and the bacterial density of L3 declines from $3.13 \times 10^9 \text{ cells g}^{-1}$ to $3.56 \times 10^8 \text{ cells g}^{-1}$. These results indicate that changes in quadrature conductivity at peak frequency are mainly associated with the bacterial density on the grain surface.

3.2. Cole-Cole Parameters Associated With Bacteria Growth and Decay

The fitted parameters related to bacteria polarization including the Cole-Cole relaxation time τ_1 , the normalized chargeability M_n^1 , the Cole-Cole exponent c_1 , the instantaneous conductivity σ_∞ , and the root mean square error (RSME) are given (see the estimated values in Tables 5, 6, and 7, for PAO1, L3, and soil without bacteria, respectively). Based on Revil, Atekwana, et al. (2012), the relaxation time is associated with the single bacterial size, and the normalized chargeability is a crucial parameter describing the magnitude of polarization. The variation of fitted Cole-Cole parameters versus bacterial density are shown in Figures 7 and 8.

During the bacterial growth and decay phases, linear relationships between normalized chargeability and bacterial density are fitted (Figure 7). For GN bacteria (PAO1), $\Delta M_n^1 = 5.72 \times 10^{-14} C_B$ is obtained for the growth phase ($R^2 = 0.93$), where ΔM_n^1 denotes the change in normalized chargeability that offset the initial responses resulted by soil, and C_B denotes the numbers of bacteria per wet soil (cells g^{-1}), and $\Delta M_n^1 = 9.76 \times 10^{-14} C_B$ for the decay phase ($R^2 = 0.99$). For the GP bacteria L3, we have $\Delta M_n^1 = 3.88 \times 10^{-14} C_B$ for the growth phase

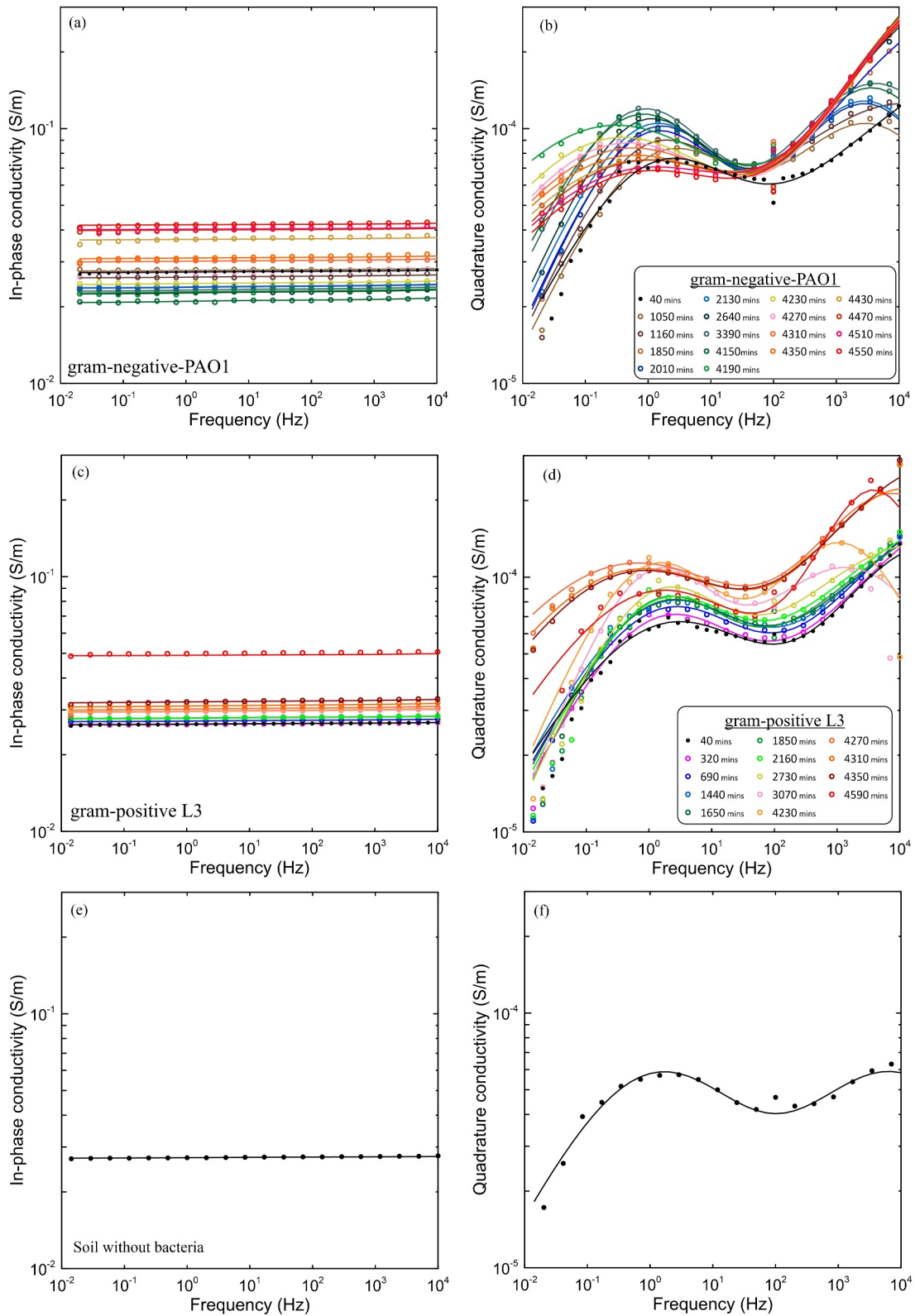


Figure 3. Quadrature and in-phase conductivity spectra during the bacterial growth and decay in the soil column experiments. The plain lines represent the best fit with a double Cole-Cole model. (a) and (b) are in-phase and quadrature conductivity for the PAO1. (c) and (d) are in-phase and quadrature conductivity for L3, respectively. (e) and (f) denote the in-phase and quadrature conductivity, respectively, for the Xinjiang soil without any bacteria.

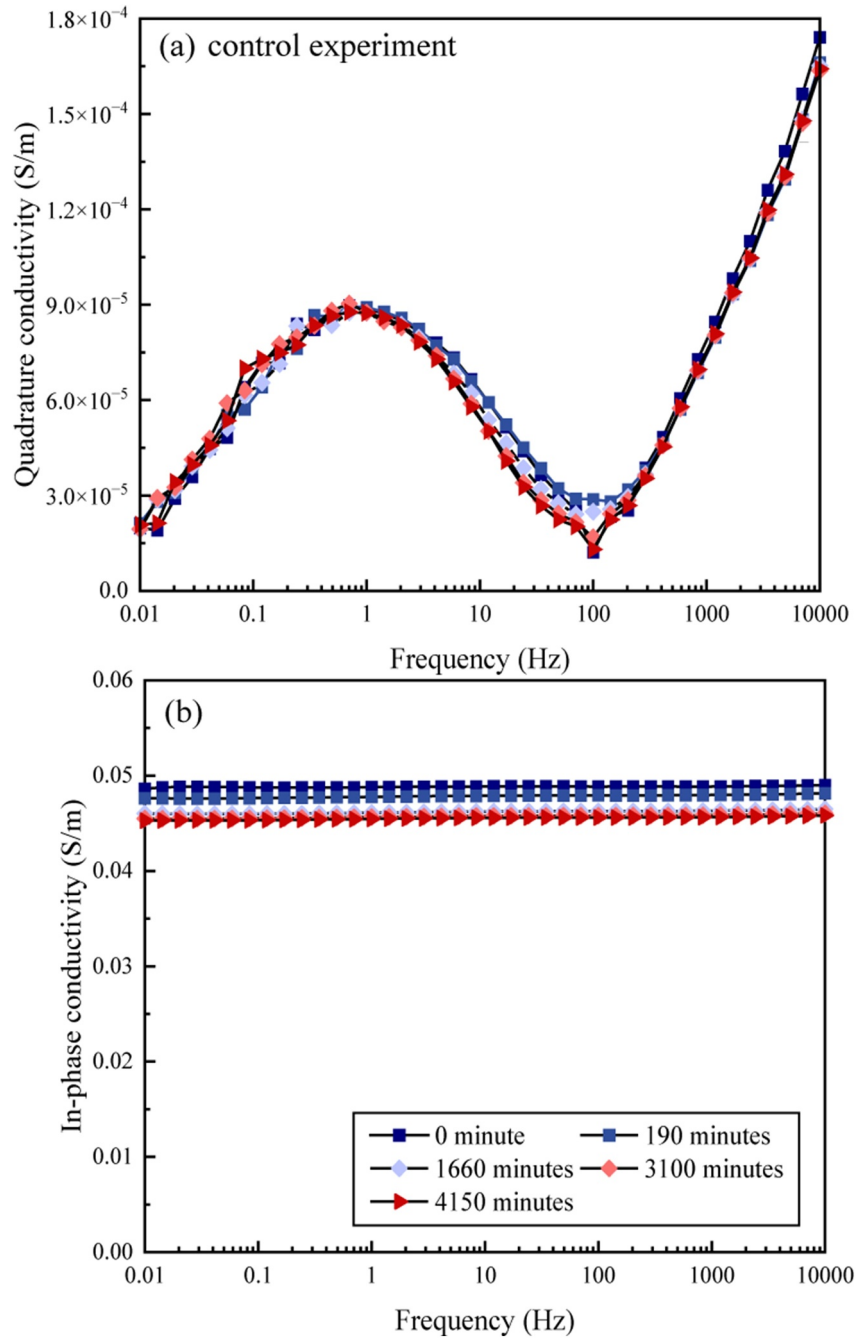


Figure 4. The quadrature (a) and in-phase conductivity (b) spectra in the control experiment (without bacteria). There is nearly no change in quadrature and in-phase conductivity with time.

($R^2 = 0.91$), and $\Delta M_n^1 = 1.54 \times 10^{-14} C_B$ for the decay phase ($R^2 = 0.99$) is obtained. Furthermore, the relaxation time is also proportional to the bacterial density during the growth and decay phases. For PAO1, we have $\tau_1 = 4.48 \times 10^{-11} C_B$ for the growth phase ($R^2 = 0.98$), and $\tau_1 = 1.28 \times 10^{-10} C_B + 0.209$ for the decay phase ($R^2 = 0.95$) is obtained. For L3, we have $\tau_1 = 1.09 \times 10^{-11} C_B + 0.085$ for the growth phase ($R^2 = 0.93$), and $\tau_1 = 1.32 \times 10^{-10} C_B + 0.08$ for the decay phase ($R^2 = 0.93$) is derived. On the contrary, the Cole-Cole exponent c_1 and the instantaneous conductivity σ_∞ are independent of bacterial density (Figure 8).

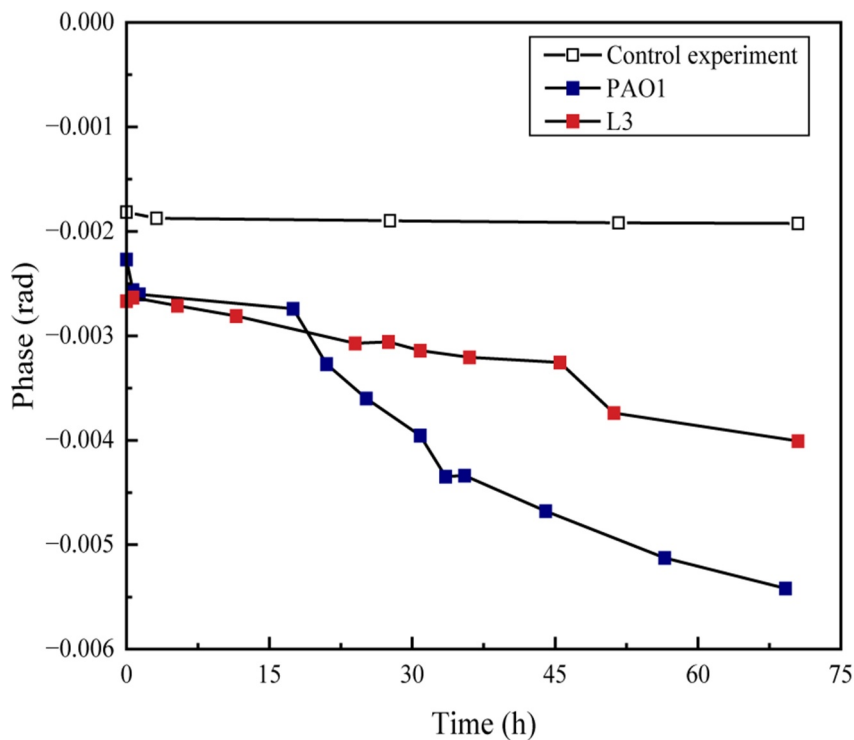


Figure 5. Evolution of the phase (1 Hz) with time in the active and control experiments. The phase changes over time in the active experiment for both PAO1 and L3, while there is no change in the control experiment.

4. Discussion

Based on the experimental results, the quadrature conductivity of bacteria in soil is primarily related to the bacterial density on the grain surface. However, whether the difference in CEC determines the variations in quadrature conductivity between different strains at the same bacterial density remains to be investigated. Furthermore, the fitting results from the double Cole-Cole model show that the normalized chargeability and relaxation time are directly influenced by bacterial density. Therefore, it is important to determine how the increase in bacterial density affects these two parameters.

4.1. SIP Response of Different Bacteria in Natural Soil

A linear relationship between the bacterial density on the grain surface and the corresponding quadrature conductivity is established (Figure 9). For both strains, the linear relationship can be expressed by the Equation $\sigma''_{(B)} = a_B C_B + \sigma''_b$, where a_B is the coefficient ($\text{S m}^{-1} \text{g cells}^{-1}$), which is associated with the characteristic of the bacteria, the a_B of PAO1 and L3 is $(1.03 \pm 0.13) \times 10^{-14}$ and $(1.22 \pm 0.22) \times 10^{-14} \text{ S m}^{-1} \text{g cells}^{-1}$, respectively. C_B is the bacterial density on the grain surface. σ''_b is the background quadrature of the mixture of soil and pore water solution. The σ''_b of PAO1 and L3 is $(7.18 \pm 0.31) \times 10^{-5}$ and $(8.45 \pm 0.45) \times 10^{-5} \text{ S m}^{-1}$, respectively. As illustrated in Figure 9, the quadrature conductivity of L3 is higher than that of PAO1 under the condition of the same bacterial density on the soil grain surface. However, the difference in quadrature conductivity between these two strains is much smaller than the difference in their CEC. For instance, at a given bacterial density of $2 \times 10^9 \text{ cells g}^{-1}$, the quadrature conductivity of L3 ($10.89 \times 10^{-5} \text{ S m}^{-1}$) is 1.2 times that of PAO1 ($9.24 \times 10^{-5} \text{ S m}^{-1}$), while the CEC of L3 is the 7.6 times that of PAO1. This phenomenon is attributed to the varying mass fractions of the bacteria, defined as the ratio of bacterial mass to the total mass of the soil (Equation 8). The dry mass of a single PAO1 bacterium is approximately 2.3 times of a single L3 bacterium (Bratbak & Dundas, 1984; Guillemin & Larson, 1922; Ross & Billing, 1957). Additionally, due to the varying growth states and structural differences of GP and GN bacteria, the wet mass of a single PAO1 bacterium may be more even greater than 2.3 times that of a single L3 bacterium (Abee & Wouters, 1999). Therefore, although the bacterial density of the two strains is identical, the significant difference in their mass fractions offsets the

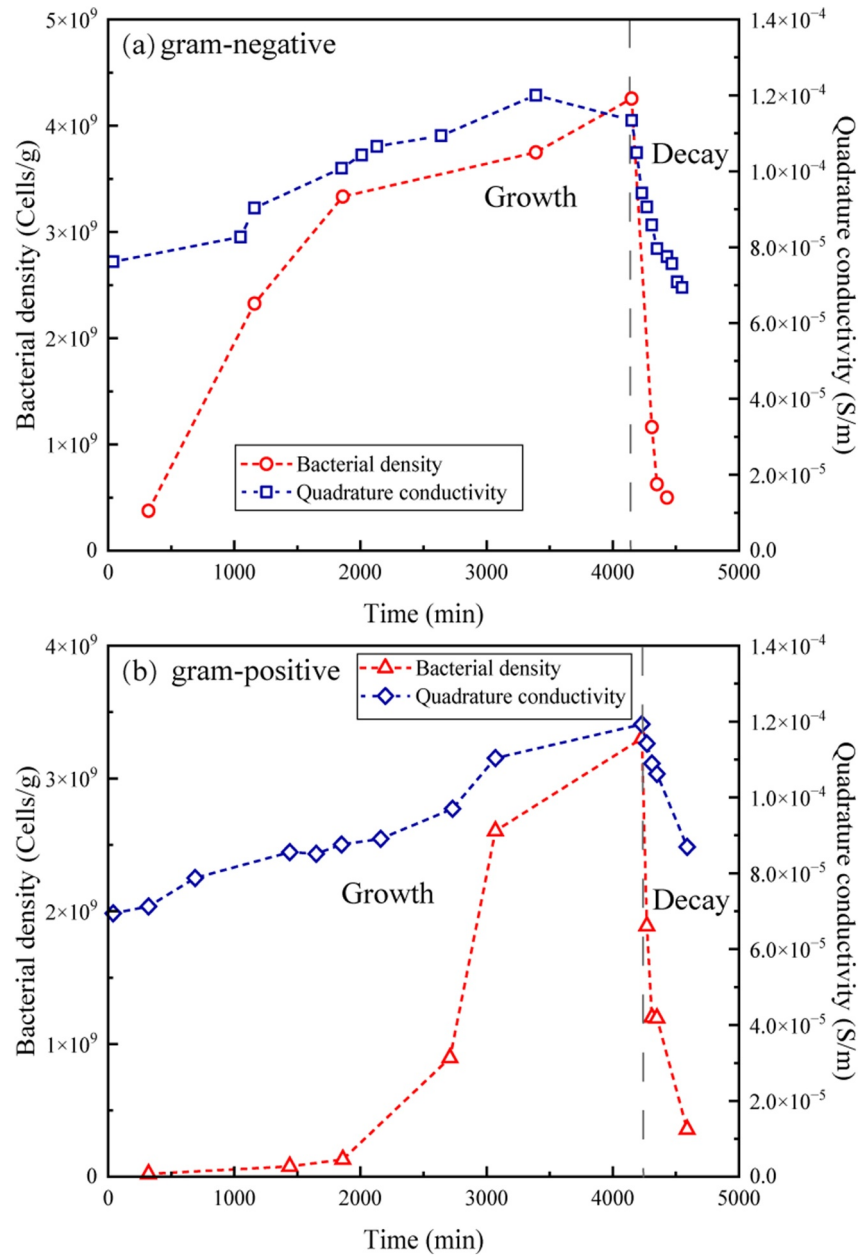


Figure 6. The variation of bacterial density and corresponding quadrature conductivity (peak frequency) during the bacterial growth and decay phases for PAO1 (a) and L3 (b), respectively. Note that the peak frequency changed from 2.89 to 0.70 Hz and 1.00 Hz for PAO1 and L3, respectively.

variation in CEC between L3 and PAO1. This indicates that the differences in the CEC of strains does not solely determine the variation in quadrature conductivity of bacteria in porous media.

4.2. Factors Affecting the Cole-Cole Parameters

As introduced in Section 2.6, the normalized chargeability of soil alone can be calculated as follows:

$$M_n^1 = \frac{s_w^{n-1}}{F} \lambda \rho_g \left[\frac{1-\phi}{\phi} \right] \varphi_C \text{CEC}_C, \quad (14)$$

Table 5
The Fitted Parameters of the Double Cole-Cole Model During PAO1 Growth and Decay

Elapsed time (minutes)	M_n^1 (S/m)	τ_1 (s)	c_1	σ_∞ (S/m)	RMSE
40	2.296×10^{-4}	0.080	0.521	0.029	0.42
1,050	3.394×10^{-4}	0.075	0.537	0.028	0.40
1,160	3.052×10^{-4}	0.118	0.582	0.027	0.28
1,860	3.498×10^{-4}	0.131	0.592	0.026	0.29
2,010	3.918×10^{-4}	0.112	0.587	0.025	0.32
2,130	4.154×10^{-4}	0.126	0.573	0.025	0.35
2,640	3.999×10^{-4}	0.161	0.593	0.025	0.32
3,390	4.757×10^{-4}	0.195	0.572	0.024	0.20
4,150	4.885×10^{-4}	0.206	0.542	0.022	0.46
4,190	6.675×10^{-4}	0.618	0.372	0.026	0.28
4,230	5.541×10^{-4}	0.493	0.396	0.027	0.21
4,270	5.156×10^{-4}	0.407	0.404	0.030	0.14
4,310	5.070×10^{-4}	0.375	0.388	0.033	0.12
4,350	4.977×10^{-4}	0.349	0.372	0.033	0.13
4,430	5.021×10^{-4}	0.258	0.354	0.039	0.15
4,470	4.751×10^{-4}	0.236	0.371	0.042	0.10
4,510	4.623×10^{-4}	0.222	0.352	0.042	0.13
4,550	4.375×10^{-4}	0.216	0.363	0.044	0.17

where the CEC of the soil is about 0.8 cmol/kg, and the porosity of the soil column is 0.35 ± 0.02 . The value of λ (Na^+ , 25°C) = $3.0 \pm 0.7 \times 10^{-10} \text{ m}^2 \text{ s}^{-1} \text{ V}^{-1}$; the ρ_g of the grain is 2650 kg/m^3 (Revil et al., 2017). When bacteria are present in the soil, the normalized chargeability is the sum of soil and bacteria and can be determined by the following equation:

Table 6
The Fitted Parameters of a Double Cole-Cole Model During L3 Growth and Decay

Elapsed time (minutes)	M_n^1 (S/m)	τ_1 (s)	c_1	σ_∞ (S/m)	RMSE
40	3.481×10^{-4}	0.070	0.442	0.027	0.33
320	2.926×10^{-4}	0.084	0.515	0.028	0.50
690	3.361×10^{-4}	0.079	0.495	0.028	0.50
1,440	3.245×10^{-4}	0.083	0.540	0.029	0.70
1,650	3.163×10^{-4}	0.088	0.528	0.029	0.33
1,850	2.923×10^{-4}	0.094	0.576	0.029	0.52
2,160	3.067×10^{-4}	0.089	0.548	0.029	0.34
2,730	3.059×10^{-4}	0.095	0.594	0.031	0.39
3,070	3.596×10^{-4}	0.115	0.638	0.030	0.32
4,230	4.286×10^{-4}	0.120	0.594	0.030	0.19
4,270	7.415×10^{-4}	0.308	0.368	0.031	0.14
4,310	6.601×10^{-4}	0.251	0.387	0.032	0.11
4,350	5.984×10^{-4}	0.265	0.406	0.034	0.17
4,590	5.043×10^{-4}	0.110	0.422	0.050	0.96

Table 7
The Fitted Parameters of a Double Cole-Cole Model of the Soil Without Bacteria

Soil type	M_n^1 (S/m)	τ_1 (s)	c_1	σ_∞ (S/m)	RMSE
Xinjiang soil	2.77×10^{-4}	0.115	0.485	0.028	0.92

Note. The pore water conductivity of the soil column is 0.1065 S m^{-1} using the BHB feeding solution.

$$M_n^1 = \frac{s_w^{n-1}}{F} \lambda \left[\frac{1-\phi}{\phi} \right] (\rho_g \phi_C \text{CEC}_C + \rho_B \phi_B \text{CEC}_B), \quad (15)$$

Two times ($t_1 = 2,640 \text{ min}$ and $t_2 = 4,150 \text{ min}$ during the PAO1 growth phase) are selected in experiments C12 and C13. The sediment formation factor F increases from 5.40 to 6.28. The CEC of the soil is measured to be 2.4 and 3.9 cmol/kg at 2,640 and 4,150 min, respectively. During the same time period, the bacterial density increases from $3.53 \times 10^9 \text{ cells g}^{-1}$ to $4.26 \times 10^9 \text{ cells g}^{-1}$. The density of PAO1 is approximately $1,100 \text{ kg m}^{-3}$ (Bratbak & Dundas, 1984). Afterward, the normalized chargeability utilizing the aforementioned parameters with Equation 15 is computed (Table 8). The calculated normalized chargeability increases from $3.83 \times 10^{-4} \text{ S m}^{-1}$ at 2,640 min to $4.84 \times 10^{-4} \text{ S m}^{-1}$ at 4,150 min. It should be noted that the porosity of soil column may have small change owing to the bacteria activity (Cui et al., 2021; Kim et al., 2010; Wang et al., 2020; Yang et al., 2021). Combining the results of bacterial density (Figure 6) and the analysis above, it is inferred that the CEC of the soil provides the direct evidence for the effect of bacterial density on normalized chargeability.

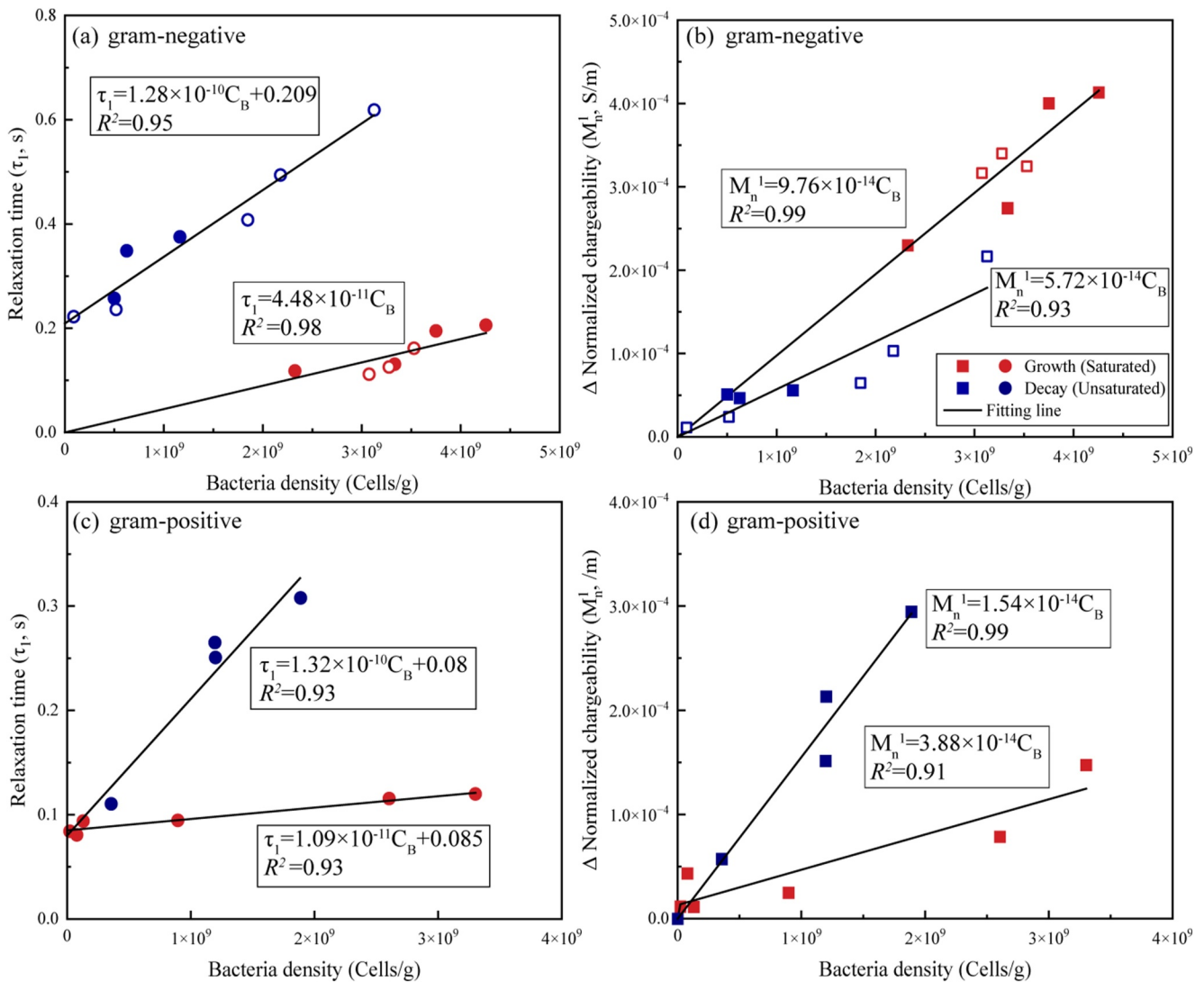


Figure 7. The relaxation time τ_1 (a and c) and change in normalized chargeability (b and d) with bacteria density for PAO1 and L3. The bacterial density was measured during the growth phase in saturated soil columns and the decay phase in unsaturated soil columns. Note that the open symbols in panels (a and b) represent bacterial density data extrapolated from the linear relationship between measured quadrature conductivity and bacteria density.

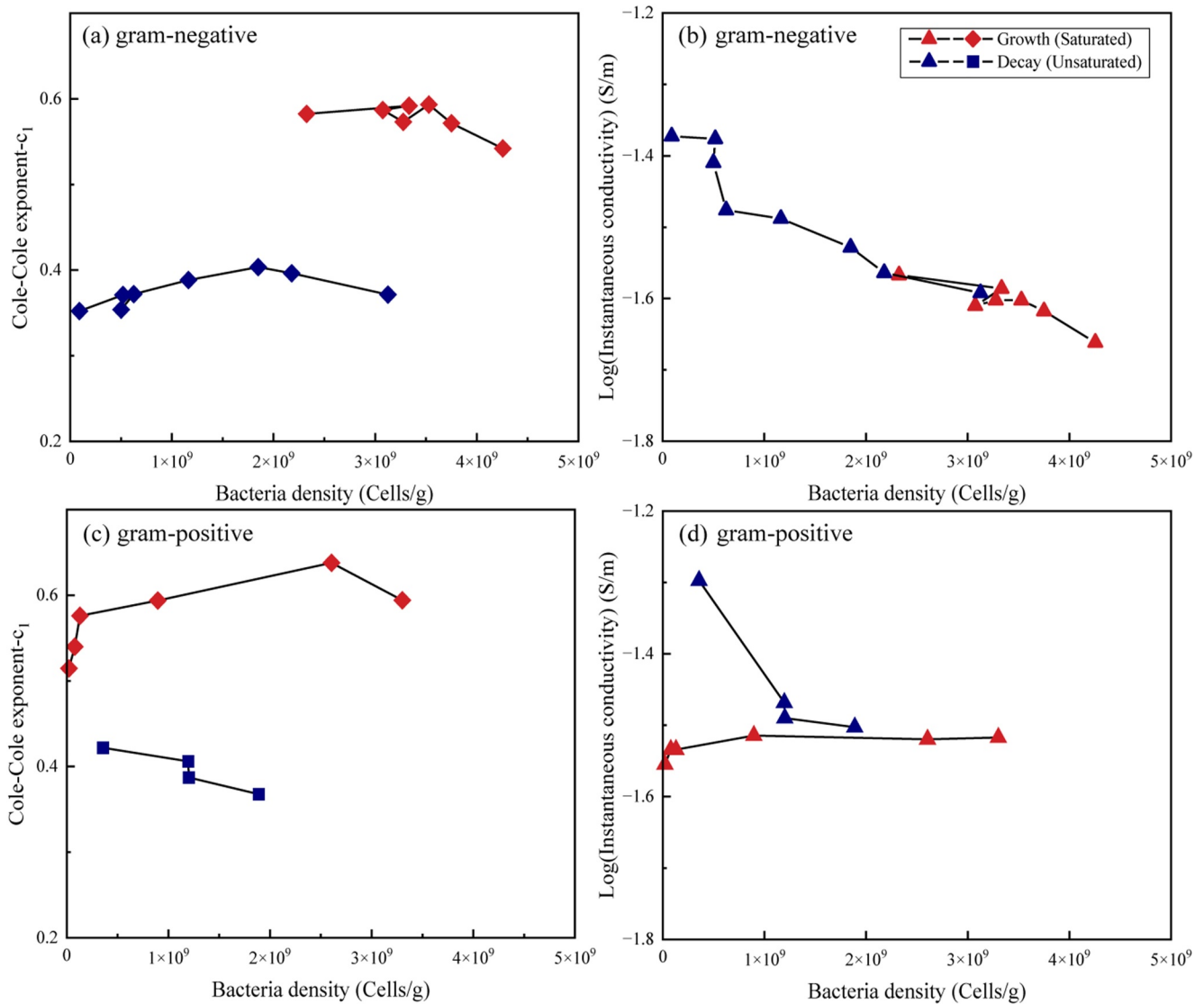


Figure 8. The variation of the low-frequency Cole-Cole exponent c_1 (a and c) and the instantaneous conductivity σ_∞ (b and d) with the bacterial density on the soil for PAO1 and L3, respectively, during the bacteria growth and decay phases. The Cole-Cole exponent c_1 and instantaneous conductivity σ_∞ show no correlation with bacteria density.

The relaxation time is an important parameter in the double Cole-Cole model. By fitting the SIP data with the double Cole-Cole model, the linear relationship between the fitted relaxation time at low frequency and bacterial density is observed. Hence, it may be inferred that the size of microcolonies attached on the soil grain surface could play a critical role in the relaxation time rather than the size of the individual bacterium when microcolonies are formed in the soil. It should be noted that increase in thickness may result from an increase in bacteria size and colony growth. To confirm this hypothesis, the SEM and CLSM technology are introduced in this study. Figures 10a and 10b shows the SEM images of PAO1 and L3. Figures 10c and 10d displays the images of microcolonies in the porous media through two stages at different magnifications. Stage 1 shows microcolonies covering the surface of the soil particles (Figure 10c); Stage 2 shows the microcolonies connections between soil particles (Figure 10d). The presence of microcolonies affects the pore structure, making it necessary to investigate whether relaxation time can be influenced by microcolonies. Therefore, dynamic changes in microcolonies thickness are detected using CLSM.

To capture the changes in microcolonies thickness during bacterial growth and decay, soil samples are destructively taken from columns at different time points. The processes of capturing microcolonies thickness

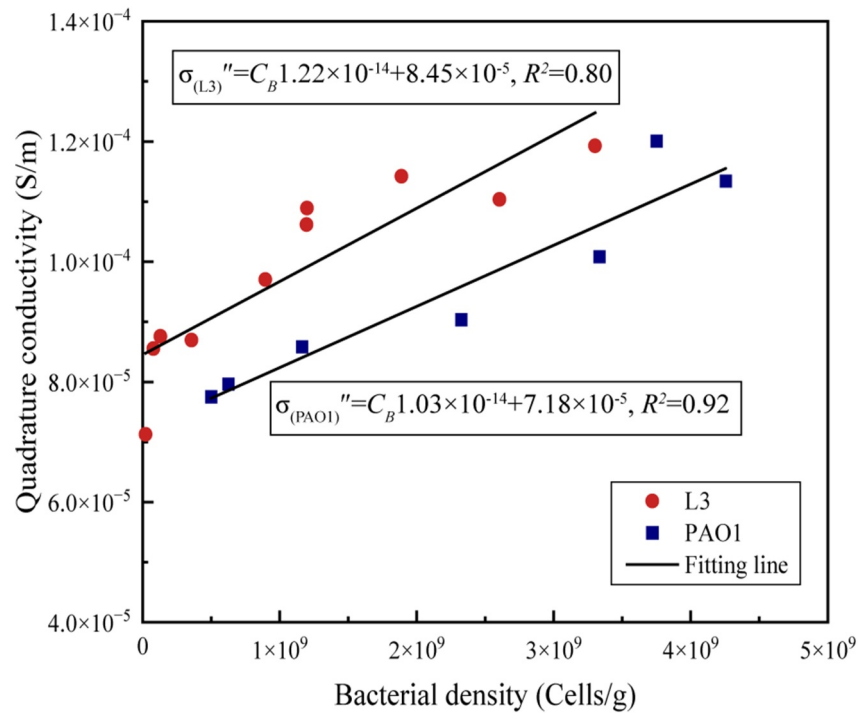


Figure 9. The linear relationship is fitted for quadrature conductivity (at the peak frequency) versus bacteria density on the soil for the two strains PAO1 and L3. The peak frequency changed from 2.89 to 0.70 Hz and 1.00 Hz for PAO1 and L3, respectively.

using CLSM are displayed in Figures 10e and 10f. The soil sample without dye under CLSM is depicted in Figure 10e, while the bacteria stained with Annexin V-FITC is displayed in Figure 10f. The step size in the z-axis of CLSM is set to 5 μm , implying that the fluorescence image is photographed by every 5 μm . The example of calculating the microcolonies thickness of samples at a location 1 cm away from the inlet of the column is given in Figure 11. The results of microcolonies thickness measurements for samples taken from different locations in the soil column at various time points during the experiments are presented in Table 9. These results are also illustrated in Figure 12 to visually observe the changes. The thickness of microcolonies vary significantly during the bacterial growth and decay phases. Taking the sample at located at 1 cm away from the inlet as an example, the thickness of microcolonies increase from 35 to 55 μm during bacterial growth phase. During the bacterial decay phase, the thicknesses of microcolonies decreases to 30 μm at 4,190 min and 22.5 μm at 4,420 min. The variations of microcolonies thicknesses at other positions in the soil column are consistent with those at 1 cm from the inlet.

Combining the results obtained from the double Cole-Cole model, the relaxation time increases with the thickening of microcolonies during the bacterial growth phase. Conversely, during the bacterial decay phase, the relaxation times decrease as the microcolonies thinned. Therefore, the thickness of the microcolonies seems to be

Table 8

Parameters Used to Calculate the Normalized Chargeability Under Different Conditions, Including the Soil Alone (Without Bacteria), and Two Elapsed Times (2,640 and 4,150 min) During the Bacterial Growth Phases

Parameters	Soil alone	2,640 min	4,150 min
CEC of the soil (cmol/kg)	0.80	2.40	3.99
F (-)	3.86	5.40	6.28
Bacterial density (cells g^{-1})	-	3.53×10^9	4.26×10^9
Normalized chargeability (S m^{-1})	2.82×10^{-4}	3.83×10^{-4}	4.84×10^{-4}

Note. F denotes the (intrinsic) formation factor.

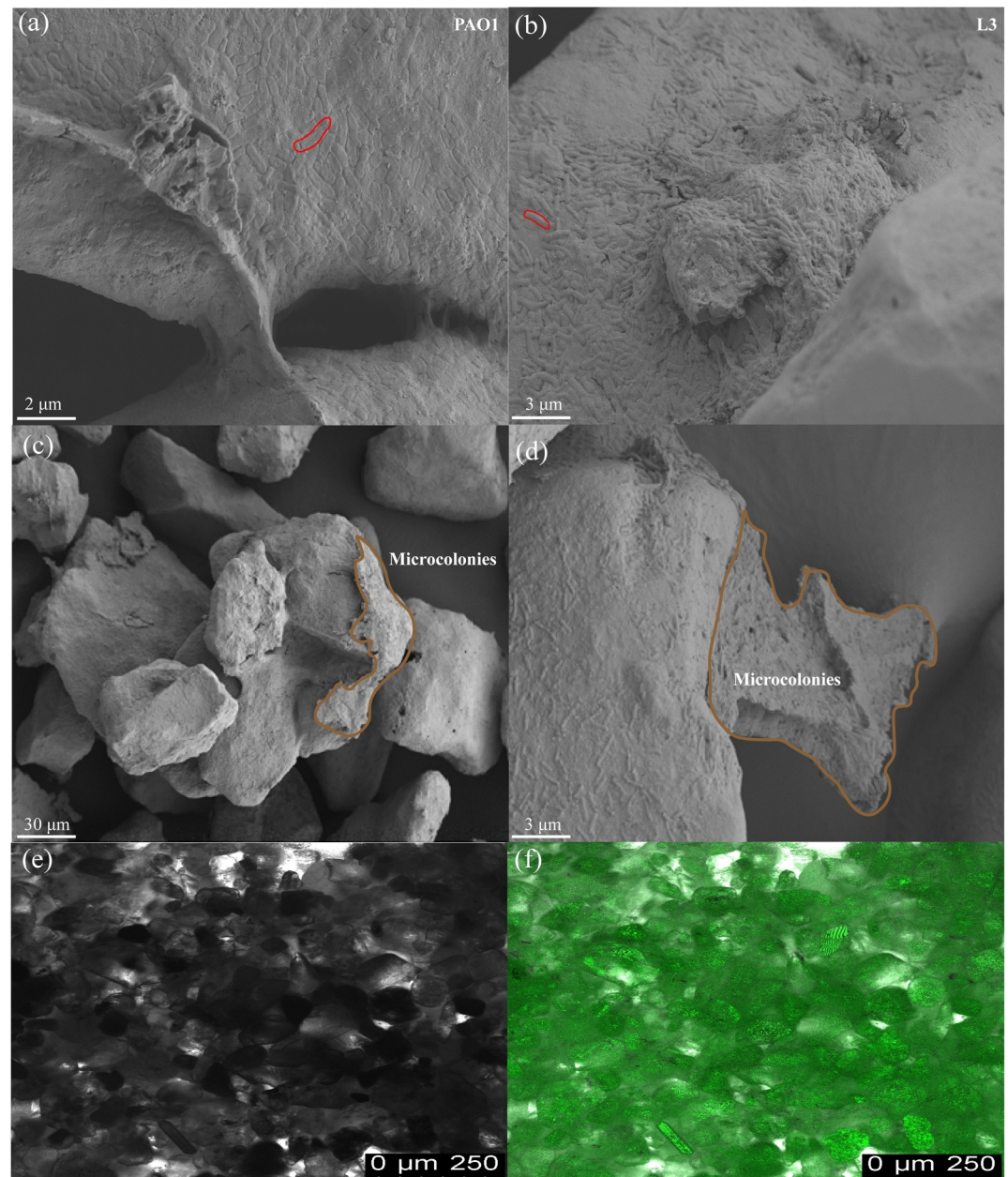


Figure 10. The scanning electron microscopy (SEM) and confocal laser scanning microscopy (CLSM) images. (a) and (b) show the SEM image of PAO1 and L3 strains. (c) Shows that microcolonies cover the surface of the soil particles; (d) shows the microcolonies connection between soil particles. (e) and (f) represent the CLSM image of soil particles without bacteria and with bacteria stained with Annexin V-FITC, respectively. The quantity of images (f) is used to calculate the microcolonies thickness on the surface of soil samples.

the key factor influencing the value of the relaxation time. A 3D sketch of the pore structure is provided in Figure 13a. The microcolonies may envelop the grain surface (Figure 13b) and connect particles through the pore space (Figure 13c). Their presence increases the polarization length thereby leading to longer relaxation times (Jougnot et al., 2010; Revil et al., 2015). Our findings regarding relaxation time differ from those of previous studies. Joo et al. (2021) conclude that the relaxation time decreases with an increase in the number of inoculated bacteria. While in this study, the change in relaxation time is attributed to the size of microcolonies. This discrepancy can be attributed to two main reasons. Firstly, the experimental conditions are different from others. The experiments are conducted to observe the growth and decay phases of bacteria in natural soils, which can

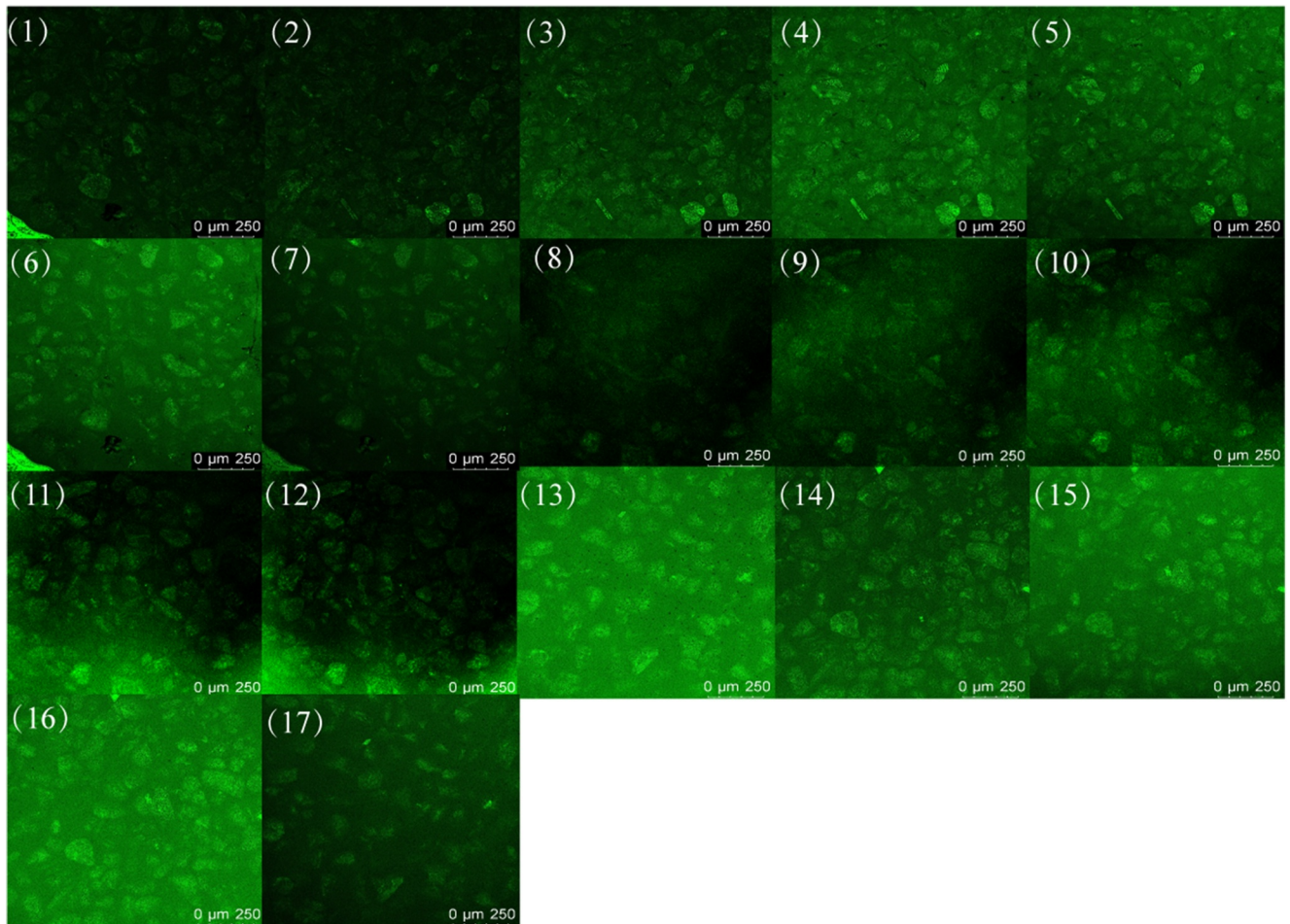


Figure 11. The fluorescence images of microcolonies under confocal laser scanning microscopy for soil samples at 1 cm away from the inlet of the column at different time intervals during bacterial growth and decay stages. Note: Images (1) to (7) and (8) to (17) represent the thicknesses of microcolonies at 1,160 and 4,150 min, respectively. The microcolonies thickness is calculated by accumulating the number of fluorescent images, multiplied by the step size (5 μm).

Table 9

The Estimated Microcolonies Thickness During the Growth and Decay at Different Positions of the Soil Column

Phases	Microcolonies thickness (growth phase, μm)		Microcolonies thickness (decay phase, μm)		
	1,160 min	4,150 min	4,190 min	4,300 min	4,420 min
1 cm	35.0	55.0	30.0	25.0	22.5
2 cm	30.0	50.0	30.0	25.0	25.0
3 cm	25.0	50.0	30.0	25.0	25.0
4 cm	25.0	50.0	30.0	25.0	22.5
5 cm	25.0	55.0	27.5	25.0	22.5
6 cm	22.5	50.0	25.0	25.0	22.5

Note. The position is 1, 2, 3, 4, 5, and 6 cm away from the inlet of the soil column. The microcolonies thickness increases with time during the bacterial growth phase, and decreases during the bacterial decay phase at all positions.

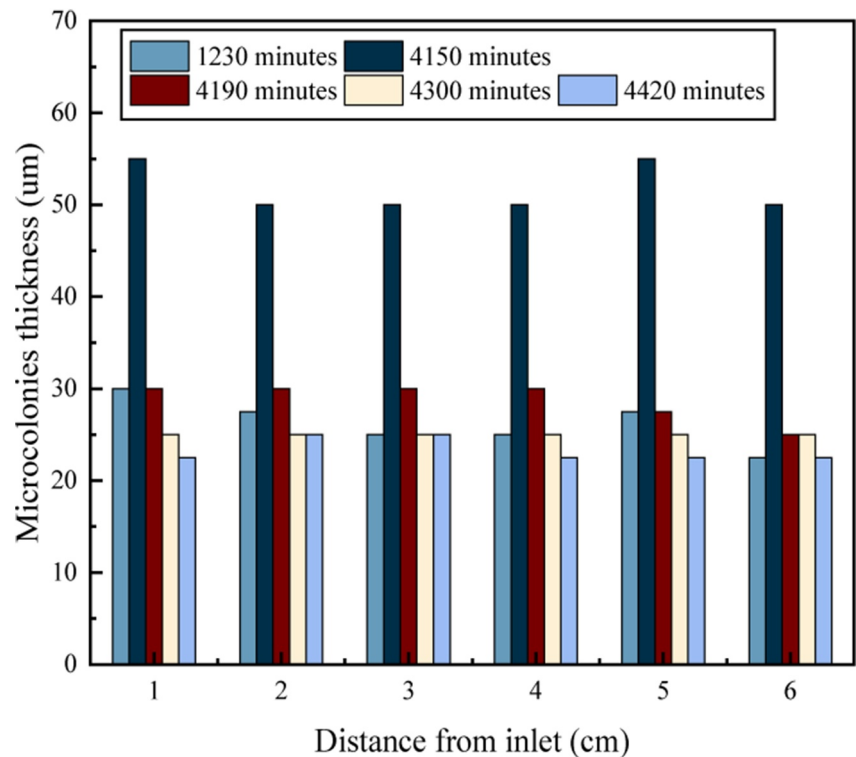


Figure 12. The variation of microcolonies thickness with the distance away from inlet of the column during bacterial growth (1,160 and 4,150 min) and the decay phase (4,190, 4,300 and 4,420 min). The microcolonies thickness increases with time during the bacterial growth phase and decreases during the bacterial decay phase at all positions.

provide more adsorption sites, and facilitate the formation of microcolonies (Bellin & Rao, 1993). Furthermore, the double Cole-Cole complex conductivity model is utilized to interpret the SIP data, which exclusively examine the low-frequency polarization caused by bacteria. Therefore, based on the results of this study, we determine that the parameter d_B in Equation 12 should refer to the size of the microcolonies, rather than the size of individual bacteria.

5. Conclusions

Soil column experiments are conducted using the SIP method to monitor the growth and decay phases of two bacterial types in a natural soil environment. The complex conductivity spectra are collected over a frequency range of 0.01–10,000 Hz. The SIP responses indicate that quadrature conductivity is directly proportional to bacterial density on the grain surface. When comparing the SIP responses of two different bacteria, it is important to consider not only the CEC and bacterial density but also the mass of individual bacterium. By fitting the SIP response with a double Cole-Cole complex conductivity model, relationships between density of bacteria in the soil and the Cole-Cole parameters can be observed. Both normalized chargeability and the relaxation time are influenced by bacterial density. Integrating the experimental results, the variation in normalized chargeability is attributed to the changes in CEC. Regarding the relaxation time, combining the results from the CLSM method, it is more likely to be affected by the size of the microcolonies rather than the size of the individual bacterium. This will remain to be explored further through numerical simulations.

This study implies that the CEC and the mass of individual bacteria are the important factors influencing the SIP response of a soil-bearing bacteria. Additionally, interpreting SIP data with the double Cole-Cole complex conductivity model can provide evidence for microbial-induced changes in porous media, thereby enhancing the applicability of this method and improving our ability to continuously observe bacterial activity and understand critical zone dynamic processes. In the future, geophysical methods can be applied to monitoring the biodegradation of organic contaminants and the immobilization of heavy metals by microorganisms in the Earth's critical zone.

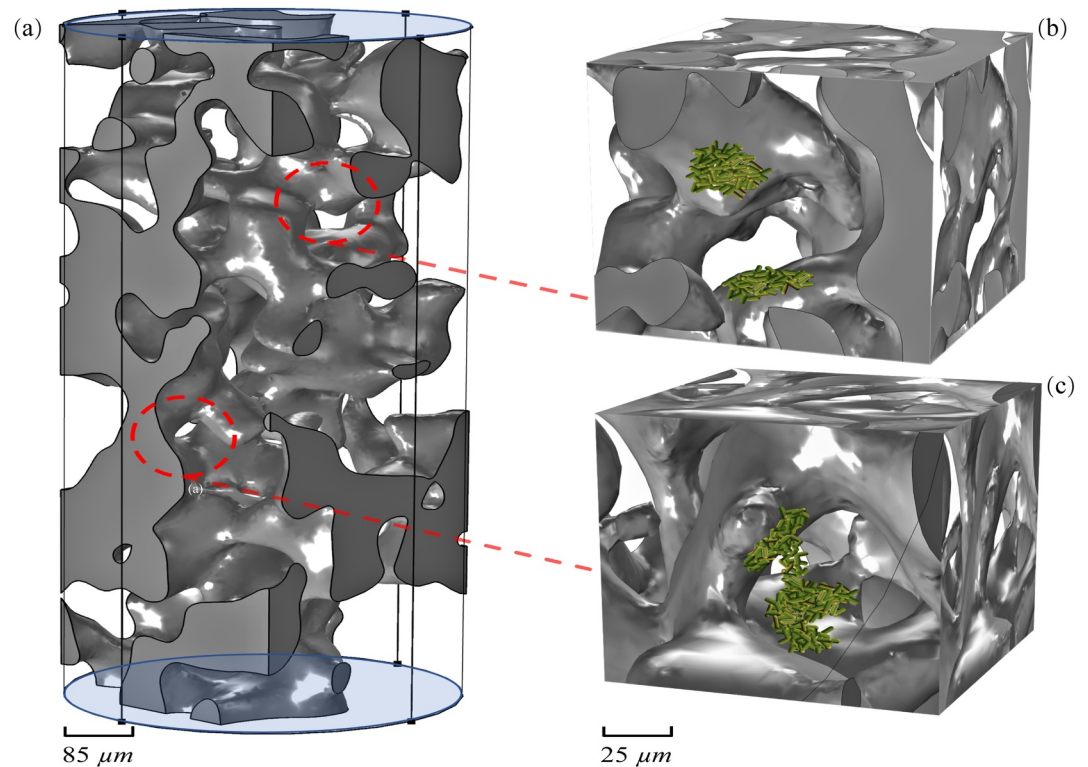


Figure 13. Three-dimensional sketch of the pore structure inside the column. (a) Pore structure of the porous media throughout the whole column. (b) and (c) show the evolution of microcolonies in the porous media through two stages, respectively. Stage 1 (b): The microcolonies are wrapped around the surface of porous media. Stage 2 (c): The microcolonies form connections between soil particle as the bacteria grow.

Data Availability Statement

The experimental data used in this study are available on [Zenodo.org](https://doi.org/10.5281/zenodo.10715864) at <https://doi.org/10.5281/zenodo.10715864> (Song et al., 2024).

Acknowledgments

This work is supported by the National Key Research and Development Program of China (2022YFC3703101) and the National Natural Science Foundation of China (42472318, 41977157, 42202267). We thank the Editor Deborah Huntzinger, the anonymous Associate Editor, and three anonymous referees for their constructive and fruitful comments to improve the quality of this work.

References

- Abdel Aal, G., Atekwana, E., Radzikowski, S., & Rossbach, S. (2009). Effect of bacterial adsorption on low frequency electrical properties of clean quartz sands and iron-oxide coated sands. *Geophysical Research Letters*, *36*(4). <https://doi.org/10.1029/2008GL036196>
- Abdel Aal, G. Z., Atekwana, E. A., & Atekwana, E. A. (2010). Effect of bioclogging in porous media on complex conductivity signatures. *Journal of Geophysical Research*, *115*(G3). <https://doi.org/10.1029/2009JG001159>
- Abdel Aal, G. Z., Atekwana, E. A., Rossbach, S., & Werkema, D. D. (2010). Sensitivity of geoelectrical measurements to the presence of bacteria in porous media. *Journal of Geophysical Research*, *115*(G3). <https://doi.org/10.1029/2009JG001279>
- Abdel Aal, G. Z., Atekwana, E. A., Slater, L. D., & Atekwana, E. A. (2004). Effects of microbial processes on electrolytic and interfacial electrical properties of unconsolidated sediments. *Geophysical Research Letters*, *31*(12). <https://doi.org/10.1029/2004GL020030>
- Abdel Aal, G. Z., Slater, L. D., & Atekwana, E. A. (2006). Induced-polarization measurements on unconsolidated sediments from a site of active hydrocarbon biodegradation. *Geophysics*, *71*(2), H13–H24. <https://doi.org/10.1190/1.2187760>
- Abee, T., & Wouters, J. A. (1999). Microbial stress response in minimal processing. *International Journal of Food Microbiology*, *50*(1–2), 65–91. [https://doi.org/10.1016/S0168-1605\(99\)00078-1](https://doi.org/10.1016/S0168-1605(99)00078-1)
- Aran, D., Maul, A., & Masfaraud, J. F. (2008). A spectrophotometric measurement of soil cation exchange capacity based on cobalhexamine chloride absorbance. *Comptes Rendus Geoscience*, *340*(12), 865–871. <https://doi.org/10.1016/j.crte.2008.07.015>
- Arumugam, T. (2017). Optimization of media components for production of antimicrobial compound by *Brevibacillus brevis* EGS9 isolated from mangrove ecosystem. *Journal of Microbiological Methods*, *142*, 83–89. <https://doi.org/10.1016/j.mimet.2017.09.010>
- Atekwana, E. A., Atekwana, E., Legall, F. D., & Krishnamurthy, R. V. (2004). Field evidence for geophysical detection of subsurface zones of enhanced microbial activity. *Geophysical Research Letters*, *31*(23). <https://doi.org/10.1029/2004GL021576>
- Atekwana, E. A., Atekwana, E. A., Rowe, R. S., Werkema, D. D., & Legall, F. D. (2004). The relationship of total dissolved solids measurements to the bulk electrical conductivity in an aquifer contaminated with hydrocarbon. *Journal of Applied Geophysics*, *56*(4), 281–294. <https://doi.org/10.1016/j.jappgeo.2004.08.003>
- Atekwana, E. A., Atekwana, E. A., Werkema, D. D., Allen, J. P., Smart, L. A., Duris, J. W., et al. (2004). Evidence for microbial enhanced electrical conductivity in hydrocarbon-contaminated sediments. *Geophysical Research Letters*, *31*(23), L23501. <https://doi.org/10.1029/2004GL021359>

- Atekwana, E. A., & Slater, L. D. (2009). Biogeophysics: A new Frontier in earth science research. *Reviews of Geophysics*, 47(4). <https://doi.org/10.1029/2009RG000285>
- Atekwana, E. A., Werkema, D. D., & Atekwana, E. A. (2006). *Biogeophysics: The effects of microbial processes on geophysical properties of the shallow subsurface* (pp. 161–193). Applied Hydrogeophysics. <https://doi.org/10.1007/978-1-4020-4912-56>
- Bellin, C. A., & Rao, P. S. C. (1993). Impact of bacterial biomass on contaminant sorption and transport in a subsurface soil. *Applied and Environmental Microbiology*, 59(6), 1813–1820. <https://doi.org/10.1128/aem.59.6.1813-1820.1993>
- Borch, T., Kretzschmar, R., Kappler, A., Cappellen, P. V., Ginder-Vogel, M., Voegelin, A., & Campbell, K. (2010). Biogeochemical redox processes and their impact on contaminant dynamics. *Environmental Science & Technology*, 44(1), 15–23. <https://doi.org/10.1021/es9026248>
- Bratbak, G., & Dundas, I. (1984). Bacterial dry matter content and biomass estimations. *Applied and Environmental Microbiology*, 48(4), 755–757. <https://doi.org/10.1128/aem.48.4.755-757.1984>
- Cen, L., Neoh, K. G., & Kang, E. T. (2004). Antibacterial activity of cloth functionalized with N-alkylated poly (4-vinylpyridine). *Journal of Biomedical Materials Research Part A: An Official Journal of The Society for Biomaterials, The Japanese Society for Biomaterials, and the Australian Society for Biomaterials and the Korean Society for Biomaterials*, 71(1), 70–80. <https://doi.org/10.1002/jbm.a.30125>
- Cheng, C., Teng, J., Xu, G., Wei, H., & Geng, C. (2024). Modelling polarization effect in electrical conductivity of frozen soil. *Cold Regions Science and Technology*, 218, 104075. <https://doi.org/10.1016/j.coldregions.2023.104075>
- Cole, K. S., & Cole, R. H. (1941). Dispersion and absorption in dielectrics I. Alternating current characteristics. *The Journal of Chemical Physics*, 9(4), 341–351. <https://doi.org/10.1063/1.1750906>
- Cui, R., Page, D., Du, X., Zhang, H., & Ye, X. (2023). Effect of iron on biological clogging in porous media: Implications for managed aquifer recharge. *Hydrological Processes*, 37(3), e14839. <https://doi.org/10.1002/hyp.14839>
- Cui, R., Ye, X., & Du, X. (2021). Coupled effects of bacteria and suspended solids on clogging during managed aquifer recharge. *Journal of Hydrology*, 600, 126543. <https://doi.org/10.1016/j.jhydrol.2021.126543>
- Davis, C. A., Atekwana, E., Atekwana, E., Slater, L. D., Rossbach, S., & Mormile, M. R. (2006). Microbial growth and biofilm formation in geologic media is detected with complex conductivity measurements. *Geophysical Research Letters*, 33(18). <https://doi.org/10.1029/2006GL027312>
- Deng, Y., Shi, X., Revil, A., Wu, J., & Ghorbani, A. (2018). Complex conductivity of oil-contaminated clayey soils. *Journal of Hydrology*, 561, 930–942. <https://doi.org/10.1016/j.jhydrol.2018.04.055>
- Deng, Y., Shi, X., Zhang, Z., Sun, Y., Wu, J., & Qian, J. (2020). Application of spectral induced polarization for characterizing surfactant-enhanced DNAPL remediation in laboratory column experiments. *Journal of Contaminant Hydrology*, 230, 103603. <https://doi.org/10.1016/j.jconhyd.2020.103603>
- Dittrich, M., & Sibling, S. (2005). Cell surface groups of two picocyanobacteria strains studied by zeta potential investigations, potentiometric titration, and infrared spectroscopy. *Journal of Colloid and Interface Science*, 286(2), 487–495. <https://doi.org/10.1016/j.jcis.2005.01.029>
- Doutereolo, I., Jackson, M., Solomon, C., & Boxall, J. (2016). Microbial analysis of in situ biofilm formation in drinking water distribution systems: Implications for monitoring and control of drinking water quality. *Applied Microbiology and Biotechnology*, 100(7), 3301–3311. <https://doi.org/10.1007/s00253-015-7155-3>
- El Alam, J., Revil, A., & Dick, P. (2023). Influence of the water content on the complex conductivity of bentonite. *Engineering Geology*, 107183, 107183. <https://doi.org/10.1016/j.enggeo.2023.107183>
- Eray, M., Mättö, M., Kaartinen, M., Andersson, L. C., & Pelkonen, J. (2001). Flow cytometric analysis of apoptotic subpopulations with a combination of Annexin V-FITC, propidium iodide, and SYTO 17. *Cytometry: The Journal of the International Society for Analytical Cytology*, 43(2), 134–142. [https://doi.org/10.1002/1097-0320\(20010201\)43:2<134::AID-CYTO1028>3.0.CO;2-L](https://doi.org/10.1002/1097-0320(20010201)43:2<134::AID-CYTO1028>3.0.CO;2-L)
- Ferris, L. E., Davey, C. L., & Kell, D. B. (1990). Evidence from its temperature dependence that the β -dielectric dispersion of cell suspensions is not due solely to the charging of a static membrane capacitance. *European Biophysics Journal*, 18(5), 267–276. <https://doi.org/10.1007/BF00188039>
- Griebler, C., & Lueders, T. (2009). Microbial biodiversity in groundwater ecosystems. *Freshwater Biology*, 54(4), 649–677. <https://doi.org/10.1111/j.1365-2427.2008.02013.x>
- Guillemin, M., & Larson, W. P. (1922). The relation between the fixed and free salts of bacteria. *The Journal of Infectious Diseases*, 31(4), 349–355. <https://doi.org/10.1093/infdis/31.4.349>
- Hadjoudja, S., Deluchat, V., & Baudu, M. (2010). Cell surface characterisation of *Microcystis aeruginosa* and *Chlorella vulgaris*. *Journal of Colloid and Interface Science*, 342(2), 293–299. <https://doi.org/10.1016/j.jcis.2009.10.078>
- Irimajiri, A., Asami, K., Ichinowatari, T., & Kinoshita, Y. (1987). Passive electrical properties of the membrane and cytoplasm of cultured rat basophil leukemia cells. I. Dielectric behavior of cell suspensions in 0.01–500 MHz and its simulation with a single-shell model. *Biochimica et Biophysica Acta (BBA) - Biomembranes*, 896(2), 203–213. [https://doi.org/10.1016/0005-2736\(87\)90181-7](https://doi.org/10.1016/0005-2736(87)90181-7)
- Jett, B. D., Hatter, K. L., Huycke, M. M., & Gilmore, M. S. (1997). Simplified agar plate method for quantifying viable bacteria. *Biotechniques*, 23(4), 648–650. <https://doi.org/10.2144/97234bm22>
- Joo, H. W., Kwon, T. H., Lee, S. R., & Wu, Y. X. (2021). Relaxation behavior in low-frequency complex conductivity of sands caused by bacterial growth and biofilm formation by *Shewanella oneidensis* under a high-salinity condition. *Geophysics*, 86(6), B389–B400. <https://doi.org/10.1190/geo2020-0213.1>
- Jougnot, D., Ghorbani, A., Revil, A., Leroy, P., & Cosenza, P. (2010). Spectral induced polarization of partially saturated clay-rocks: A mechanistic approach. *Geophysical Journal International*, 180(1), 210–224. <https://doi.org/10.1111/j.1365-246X.2009.04426.x>
- Kim, J. W., Choi, H., & Pachepsky, Y. A. (2010). Biofilm morphology as related to the porous media clogging. *Water Research*, 44(4), 1193–1201. <https://doi.org/10.1016/j.watres.2009.05.049>
- Kimak, C., Ntarlagiannis, D., Slater, L. D., Atekwana, E. A., Beaver, C. L., Rossbach, S., & Ustra, A. (2019). Geophysical monitoring of hydrocarbon biodegradation in highly conductive environments. *Journal of Geophysical Research: Biogeosciences*, 124(2), 353–366. <https://doi.org/10.1029/2018JG004561>
- Leone, L., Ferri, D., Manfredi, C., Persson, P., Shchukarev, A., Sjöberg, S., & Loring, J. (2007). Modeling the acid–base properties of bacterial surfaces: A combined spectroscopic and potentiometric study of the gram-positive bacterium *Bacillus subtilis*. *Environmental Science & Technology*, 41(18), 6465–6471. <https://doi.org/10.1021/es070996e>
- Leroy, P., & Revil, A. (2009). A mechanistic model for the spectral induced polarization of clay materials. *Journal of Geophysical Research*, 114(B10). <https://doi.org/10.1029/2008JB006114>
- Martin, T., Weller, A., & Behling, L. (2022). Desaturation effects of pyrite–sand mixtures on induced polarization signals. *Geophysical Journal International*, 228(1), 275–290. <https://doi.org/10.1093/gji/ggab333>
- McCarty, P. L., Reinhard, M., & Rittmann, B. E. (1981). Trace organics in groundwater. *Environmental Science & Technology*, 15(1), 40–51. <https://doi.org/10.1021/es00083a003>

- Mellage, A., Smeaton, C. M., Furman, A., Atekwana, E. A., Rezanezhad, F., & Cappellen, P. V. (2018). Linking spectral induced polarization (SIP) and subsurface microbial processes: Results from sand column incubation experiments. *Environmental Science & Technology*, 52(4), 2081–2090. <https://doi.org/10.1021/acs.est.7b04420>
- Mellage, A., Smeaton, C. M., Furman, A., Atekwana, E. A., Rezanezhad, F., & Cappellen, P. V. (2019). Bacterial stern layer diffusion: Experimental determination with spectral induced polarization and sensitivity to nitrite toxicity. *Near Surface Geophysics*, 17(6), 623–635. <https://doi.org/10.1002/nsg.12058>
- Ntarlagiannis, D., Yee, N., & Slater, L. D. (2005). On the low-frequency electrical polarization of bacterial cells in sands. *Geophysical Research Letters*, 32(24), 2–5. <https://doi.org/10.1029/2005GL024751>
- Okay, G., Leroy, P., Ghorbani, A., Cosenza, P., Camerlynck, C., Cabrera, J., et al. (2014). Spectral induced polarization of clay-sand mixtures: Experiments and modeling. *Geophysics*, 79(6), E353–E375. <https://doi.org/10.1190/geo2013-0347.1>
- Oldham, K. B. (2008). A Gouy–Chapman–Stern model of the double layer at a (metal)/(ionic liquid) interface. *Journal of Electroanalytical Chemistry*, 613(2), 131–138. <https://doi.org/10.1016/j.jelechem.2007.10.017>
- Olhoeft, G. R. (1985). Low-frequency electrical properties. *Geophysics*, 50(12), 2492–2503. <https://doi.org/10.1190/1.1441880>
- Orozco, A. F., Ciampi, P., Katona, T., Censini, M., Papini, M. P., Deidda, G. P., & Cassiani, G. (2021). Delineation of hydrocarbon contaminants with multi-frequency complex conductivity imaging. *Science of the Total Environment*, 768, 144997. <https://doi.org/10.1016/j.scitotenv.2021.144997>
- Orozco, A. F., Velimirovic, M., Tosco, T., Kemna, A., Sapion, H., Klaas, N., et al. (2015). Monitoring the injection of microscale zerovalent iron particles for groundwater remediation by means of complex electrical conductivity imaging. *Environmental Science & Technology*, 49(9), 5593–5600. <https://doi.org/10.1021/acs.est.5b00208>
- Panwar, N., Revil, A., Sharma, R., Schmutz, M., Duvillard, P. A., Garcia, B., et al. (2021). Induced polarization of carbonates. *Journal of Geophysical Research: Solid Earth*, 126(6), e2021JB022029. <https://doi.org/10.1029/2021JB022029>
- Personna, Y. R., Slater, L., Ntarlagiannis, D., Werkema, D., & Szabo, Z. (2013). Complex resistivity signatures of ethanol biodegradation in porous media. *Journal of Contaminant Hydrology*, 153, 37–50. <https://doi.org/10.1016/j.jconhyd.2013.07.005>
- Poortinga, A. T., Bos, R., Norde, W., & Busscher, H. J. (2002). Electric double layer interactions in bacterial adhesion to surfaces. *Surface Science Reports*, 47(1), 1–32. [https://doi.org/10.1016/S0167-5729\(02\)00032-8](https://doi.org/10.1016/S0167-5729(02)00032-8)
- Revil, A. (2012). Spectral induced polarization of shaly sands: Influence of the electrical double layer. *Water Resources Research*, 48(2), W02517. <https://doi.org/10.1029/2011WR011260>
- Revil, A. (2013). Effective conductivity and permittivity of unsaturated porous materials in the frequency range 1 mHz–1GHz. *Water Resources Research*, 49(1), 306–327. <https://doi.org/10.1029/2012WR012700>
- Revil, A., Atekwana, E., Zhang, C., Jardani, A., & Smith, S. (2012). A new model for the spectral induced polarization signature of bacterial growth in porous media. *Water Resources Research*, 48(9). <https://doi.org/10.1029/2012WR011965>
- Revil, A., Binley, A., Mejus, L., & Kessouri, P. (2015). Predicting permeability from the characteristic relaxation time and intrinsic formation factor of complex conductivity spectra. *Water Resources Research*, 51(8), 6672–6700. <https://doi.org/10.1002/2015WR017074>
- Revil, A., Coperey, A., Deng, Y., Cerepi, A., & Seleznev, N. (2018). Complex conductivity of tight sandstones. *Geophysics*, 83(2), E55–E74. <https://doi.org/10.1190/GEO2017-0096.1>
- Revil, A., Coperey, A., Shao, Z., Florsch, N., Fabricius, I. L., Deng, Y., et al. (2017). Complex conductivity of soils. *Water Resources Research*, 53(8), 7121–7147. <https://doi.org/10.1002/2017WR020655>
- Revil, A., Eppehimer, J. D., Skold, M., Karaoulis, M., Godinez, L., & Prasad, M. (2013). Low-frequency complex conductivity of sandy and clayey materials. *Journal of Colloid and Interface Science*, 398, 193–209. <https://doi.org/10.1016/j.jcis.2013.01.015>
- Revil, A., Florsch, N., & Camerlynck, C. (2014). Spectral induced polarization porosimetry. *Geophysical Journal International*, 198(2), 1016–1033. <https://doi.org/10.1093/gji/ggu180>
- Revil, A., Ghorbani, A., Jougnot, D., & Yven, B. (2023). Induced polarization of clay-rich materials—Part 1: The effect of desiccation. *Geophysics*, 88(4), MR195–MR210. <https://doi.org/10.1190/geo2022-0510.1>
- Revil, A., Ghorbani, A., Jougnot, D., Yven, B., Grgic, D., Bretaudeau, F., & Deparis, J. (2023). Induced polarization of clay-rich materials—Part 2: The effect of anisotropy. *Geophysics*, 88(6), MR305–MR322. <https://doi.org/10.1190/geo2022-0511.1>
- Revil, A., Karaoulis, M., Johnson, T., & Kemna, A. (2012). Review: Some low-frequency electrical methods for subsurface characterization and monitoring in hydrogeology. *Hydrogeology Journal*, 20(4), 617–658. <https://doi.org/10.1007/s10040-011-0819-x>
- Revil, A., Razdan, M., Julien, S., Coperey, A., Abdulsamad, F., Ghorbani, A., et al. (2019). Induced polarization response of porous media with metallic particles—Part 9: Influence of permafrost/Induced polarization. *Geophysics*, 84(5), E337–E355. <https://doi.org/10.1190/geo2019-0013.1>
- Revil, A., Schmutz, M., Abdulsamad, F., Balde, A., Beck, C., Ghorbani, A., & Hubbard, S. S. (2021). Field-scale estimation of soil properties from spectral induced polarization tomography. *Geoderma*, 403, 115380. <https://doi.org/10.1016/j.geoderma.2021.115380>
- Rosier, C. L., Atekwana, E. A., Abdel Aal, G., & Patrauchan, M. A. (2019). Cell concentrations and metabolites enhance the SIP response to biofilm matrix components. *Journal of Applied Geophysics*, 160, 183–194. <https://doi.org/10.1016/j.jappgeo.2018.10.023>
- Ross, K. F. A., & Billing, E. V. E. (1957). The water and solid content of living bacterial spores and vegetative cells as indicated by refractive index measurements. *Microbiology*, 16(2), 418–425. <https://doi.org/10.1099/00221287-16-2-418>
- Sanchis, A., Brown, A. P., Sancho, M., Martinez, G., Sebastian, J. L., Munoz, S., & Miranda, J. M. (2007). Dielectric characterization of bacterial cells using dielectrophoresis. *Bioelectromagnetics*, 28(5), 393–401. <https://doi.org/10.1002/bem.20317>
- Saneiyani, S., & Slater, L. (2021). Complex conductivity porosimetry during unconfined soil compression. In *First international meeting for applied geoscience and energy* (pp. 1971–1975). Society of Exploration Geophysicists. <https://doi.org/10.1190/segam2021-3578248.1>
- Schultz, P., & Urban, N. R. (2008). Effects of bacterial dynamics on organic matter decomposition and nutrient release from sediments: A modeling study. *Ecological Modelling*, 210(1–2), 1–14. <https://doi.org/10.1016/j.ecolmodel.2007.06.026>
- Schwartz, N., & Furman, A. (2012). Spectral induced polarization signature of soil contaminated by organic pollutant: Experiment and modeling. *Journal of Geophysical Research*, 117(B10). <https://doi.org/10.1029/2012JB009543>
- Sen, T. K. (2011). Processes in pathogenic biocolloidal contaminants transport in saturated and unsaturated porous media: A review. *Water, Air, and Soil Pollution*, 216(1–4), 239–256. <https://doi.org/10.1007/s11270-010-0531-9>
- Shephard, J., McQuillan, A. J., & Bremer, P. J. (2008). Mechanisms of cation exchange by *Pseudomonas aeruginosa* PAO1 and PAO1 wBpL, a strain with a truncated lipopolysaccharide. *Applied and Environmental Microbiology*, 74(22), 6980–6986. <https://doi.org/10.1128/AEM.01117-08>
- Song, Y., Shi, X., Revil, A., Ghorbani, A., Qiang, S., Xing, K., et al. (2024). Spectral induced polarization response of bacteria growth and decay in soil column experiments [Dataset]. *Zenodo*. <https://doi.org/10.5281/zenodo.10715864>

- Song, Y., Shi, X., Revil, A., & Kang, X. (2022). Monitoring in situ microbial growth and decay in soil column experiments by induced polarization. *Geophysical Research Letters*, *49*(16), e2021GL097553. <https://doi.org/10.1029/2021GL097553>
- Stevik, T. K., Aa, K., Ausland, G., & Hanssen, J. F. (2004). Retention and removal of pathogenic bacteria in wastewater percolating through porous media: A review. *Water Research*, *38*(6), 1355–1367. <https://doi.org/10.1016/j.watres.2003.12.024>
- Strobel, C., Abramov, S., Huisman, J. A., Cirkpa, O. A., & Mellage, A. (2023). Spectral Induced Polarization (SIP) of denitrification-driven microbial activity in column experiments packed with calcareous aquifer sediments. *Journal of Geophysical Research: Biogeosciences*, *128*(1), e2022JG007190. <https://doi.org/10.1029/2022JG007190>
- Takenaka, S., Iwaku, M., & Hoshion, E. (2001). Artificial *Pseudomonas aeruginosa* biofilms and confocal laser scanning microscopic analysis. *Journal of Infection and Chemotherapy*, *7*(2), 87–92. <https://doi.org/10.1007/s101560100014>
- Tan, D., Long, J., Li, B., Ding, D., Du, H., & Lei, M. (2018). Fraction and mobility of antimony and arsenic in three polluted soils: A comparison of single extraction and sequential extraction. *Chemosphere*, *213*, 533–540. <https://doi.org/10.1016/j.chemosphere.2018.09.089>
- Tong, M., Long, G., Jiang, X., & Kim, H. N. (2010). Contribution of extracellular polymeric substances on representative gram negative and gram positive bacterial deposition in porous media. *Environmental Science & Technology*, *44*(7), 2393–2399. <https://doi.org/10.1021/es9027937>
- Torrella, F., & Morita, R. Y. (1981). Microcultural study of bacterial size changes and microcolony and ultramicrocolony formation by heterotrophic bacteria in seawater. *Applied and Environmental Microbiology*, *41*(2), 518–527. <https://doi.org/10.1128/aem.41.2.518-527.1981>
- Van der Wal, A., Minor, M., Norde, W., Zehnder, A. J., & Lyklema, J. (1997). Electrokinetic potential of bacterial cells. *Langmuir*, *13*(2), 165–171. <https://doi.org/10.1021/a960386k>
- Vanhala, H., Soininen, H., & Kukkonen, I. (1992). Detecting organic chemical contaminants by spectral-induced polarization method in glacial till environment. *Geophysics*, *57*(8), 1014–1017. <https://doi.org/10.1190/1.1443312>
- Vinegar, H. J., & Waxman, M. H. (1984). Induced polarization of shaly sands. *Geophysics*, *49*(8), 1267–1287. <https://doi.org/10.1190/1.1441755>
- Walker, S. L., Hill, J. E., Redman, J. A., & Elimelech, M. (2005). Influence of growth phase on adhesion kinetics of *Escherichia coli* D21g. *Applied and Environmental Microbiology*, *71*(6), 3093–3099. <https://doi.org/10.1128/AEM.71.6.3093-3099.2005>
- Wang, H., Xin, J., Zheng, X., Li, M., Fang, Y., & Zheng, T. (2020). Clogging evolution in porous media under the coexistence of suspended particles and bacteria: Insights into the mechanisms and implications for groundwater recharge. *Journal of Hydrology*, *582*, 124554. <https://doi.org/10.1016/j.jhydrol.2020.124554>
- Weller, A., Slater, L., & Nordsiek, S. (2013). On the relationship between induced polarization and surface conductivity: Implications for petrophysical interpretation of electrical measurements. *Geophysics*, *78*(5), D315–D325. <https://doi.org/10.1190/geo2013-0076.1>
- Xu, M., Dai, W., Zhao, Z., Zheng, J., Huang, F., Mei, C., et al. (2022). Effect of rice straw biochar on three different levels of Cd-contaminated soils: Cd availability, soil properties, and microbial communities. *Chemosphere*, *301*, 134551. <https://doi.org/10.1016/j.chemosphere.2022.134551>
- Yang, Y., Wu, Y., Lu, Y., Shi, M., & Chen, W. (2021). Microorganisms and their metabolic activities affect seepage through porous media in groundwater artificial recharge systems: A review. *Journal of Hydrology*, *598*, 126256. <https://doi.org/10.1016/j.jhydrol.2021.126256>
- Zhang, C., Revil, A., Fujita, Y., Munakata-Marr, J., & Redden, G. (2014). Quadrature conductivity: A quantitative indicator of bacterial abundance in porous media. *Geophysics*, *79*(6), D363–D375. <https://doi.org/10.1190/geo2014-0107.1>
- Zhao, K., Tseng, B. S., Beckerman, B., Jin, F., Gibiansky, M. L., Harrison, J. J., et al. (2013). Psl trails guide exploration and microcolony formation in *Pseudomonas aeruginosa* biofilms. *Nature*, *497*(7449), 388–391. <https://doi.org/10.1038/nature12155>